Near-Infrared Adaptive Optics Imaging of the Central Regions of Nearby Sc Galaxies. II. NGC 247 and NGC 2403

T. J. Davidge [1, 2]
Canadian Gemini Office, Herzberg Institute of Astrophysics,
National Research Council of Canada, 5071 W. Saanich Road,
Victoria, B.C. Canada V9E 2E7
email:tim.davidge@nrc.ca

S. Courteau [1]
Herzberg Institute of Astrophysics,
National Research Council of Canada, 5071 W. Saanich Road,
Victoria, B.C. Canada V9E 2E7

and

Department of Physics & Astronomy, University of British Columbia,
Vancouver, B. C. Canada V6T 1Z1
email:courteau@astro.ubc.ca

ABSTRACT

J, H, and K' images obtained with the Canada-France-Hawaii Telescope adaptive optics system are used to investigate the star-forming histories of the central regions of the Sc galaxies NGC 247 and NGC 2403. The brightest resolved red stars within 15 arcsec of the nucleus of each galaxy are red supergiants (RSGs), indicating that the central few hundred parsecs of these galaxies experienced star formation within the last ~ 0.1 Gyr. While there are indications of galaxy-to-galaxy differences in the recent ($t \leq 0.1$ Gyr) star-forming histories, a comparison of the K luminosity functions of stars near the centers of NGC 2403 and M33 indicate that, when averaged over Gyr time scales, the star-forming histories of the inner disks of these galaxies have

[1]Visiting Astronomer, Canada-France-Hawaii Telescope Corporation, which is run by the National Research Council of Canada, the Centre National de la Recherche Scientifique, and the University of Hawaii.

[2]Guest User, Canadian Astronomy Data Centre, which is operated by the Herzberg Institute of Astrophysics, National Research Council of Canada.

been remarkably similar. This is consistent with suggestions that the long-term evolution of disks is defined by local characteristics such as mass density. It is demonstrated that NGC 247 and NGC 2403, like M33, harbour nuclear star clusters with stellar contents that differ from the surrounding central light concentrations, which in turn have near-infrared spectral energy distributions that are similar to old stellar systems. The nucleus of NGC 2403 is significantly bluer than that of the other two galaxies. If the nuclei of NGC 247, NGC 2403, and M33 are subject to similar amounts of extinction then this indicates that NGC 2403 harbours the youngest nuclear star cluster in the sample. The $K-$band surface brightnesses near the centers of NGC 247 and NGC 2403 are 1 – 2 mag arcsec^{-2} lower than in M33. Finally, it is noted that young or intermediate-age nuclear star clusters are a common occurence in nearby spirals, indicating that nuclear star formation in these objects is either continuous or episodic on time scales of $0.1 - 1$ Gyr. This is consistent with models that have been proposed to explain the properties of the Galactic Center.

Subject headings: galaxies: individual (NGC 247, NGC 2403) - galaxies: evolution - galaxies: stellar content - galaxies: bulges - galaxies: nuclei

1. INTRODUCTION

The bulges of spiral galaxies are not monolithic entities that evolve in isolation; rather, the evolution of these systems is influenced by their environment. As a reservoir containing significant quantities of gas, the disk might be expected to play a significant role in bulge evolution, and the large-scale structural characteristics of spiral galaxies provide evidence supporting a bulge-disk connection, in the sense that the impact of the disk on bulge properties becomes more important towards progressively later morphological types (Andredakis, Peletier, & Balcells 1995; Courteau, de Jong, & Broeils 1996). Interactions with the disk could explain the differences in central structural properties noted between the bulges of spirals spanning a range of morphological types (e.g. Phillips et al. 1996; Courteau 1997), as well as the presence of sub-structures (Carollo, Stiavelli, & Mack 1998) and nearly exponential light profiles (Courteau 1997; Carollo 1999; MacArthur et al. 2002) in many bulges. Physical processes that can trigger the motion of disk material into the central regions of galaxies include bar instabilities (Friedli & Benz 1993, 1995; Sellwood & Moore 1999), galaxy-galaxy interactions (Barnes & Hernquist 1992, Mihos & Hernquist 1996), and dynamical friction (Noguchi 1999, 2000).

The bulges of spiral galaxies earlier than Sc appear to be dominated by old stars, suggesting that any recent interactions with the disk (1) have been modest, and (2) have not affected the basic properties of these systems. The colors of bulges in the Hubble Deep Field indicate that these objects formed at high redshift (Abraham et al. 1999), while the tight relation in the $(B-I, I-H)$ diagram defined by the bulges of nearby early-type spirals is consistent with both a modest age spread and an old age (Peletier et al. 1999). The spectral energy distributions (SEDs) of the bulges of M31 and M81, which are the two closest intermediate-type spirals, indicate that these systems are dominated by stars that formed during early epochs (Davidge 1997, 2001b; Bica, Alloin, & Schmidt 1990; Kong et al. 2000). These observations are consistent with galaxy formation simulations, which predict that the main bodies of bulges form at $z > 2$ (e.g. Katz 1992; Steinmetz & Mueller 1994; Mollá, Ferrini, & Gozzi 2000; Gnedin, Norman, & Ostriker 2000), although star formation may continue into more recent epochs (Mollá et al. 2000). The collisionless accretion of satellites can also reproduce the observed structural characteristics of bulges, and these models also predict relatively old bulges, as the accretion must predate the formation of the thin disk (Aguerri, Balcells, & Peletier 2001).

The Milky-Way is a barred (e.g. Blitz & Spergel 1991; Dwek et al. 1995) intermediate-type (Blanco & Terndrup 1989) spiral galaxy. The Galactic bulge is of fundamental importance as an age calibrator since individual main sequence stars can be resolved. The Galactic bulge has a global mass-to-light ratio that is similar to the M31 bulge (Kent 1992), and so the bulges of the Galaxy and M31 ought to have similar stellar contents. After accounting for contamination from stars in the intervening disk, the main sequence turn-off of the Galactic bulge is indicative of an old age (Feltzing & Gilmore 2000). This is consistent with studies of bulge globular clusters (Minniti 1995), which have ages of at least ~ 10 Gyr (Ortolani et al. 1995; Chaboyer et al. 2000), although metallicity-dependent calibration issues frustrate efforts to determine when these clusters formed with respect to clusters in the outer halo (Rosenberg et al. 1999). Finally, further constraints on the age of the Galactic bulge can be obtained from the age of the Galactic disk, as the disk is expected to be one of the last components of the Galaxy to form. Using the kinematic properties of main sequence and sub-giant branch stars selected using Hipparcos information, Binney, Dehnen, & Bertelli (2000) find that the disk has an age of 11.2 ± 0.75 Gyr, and is only ~ 1 Gyr younger than the bulk of globular clusters.

Although the main bodies of bulges in early and intermediate-type spiral galaxies are dominated by old stars, the innermost regions of these objects contain young or intermediate-age stars, indicating that star formation continued to recent epochs. There are young star clusters near the Galactic Center (GC; e.g. Cotera et al. 1996), and these are in the process of being tidally disrupted (Figer et al. 1999). The youngest stars near the GC

have solar-like Fe abundances, and a metallicity distribution function that differs from that of older stars in the bulge, but is similar to that of solar-neighborhood giants (Ramirez et al. 2000), ostensibly suggesting – but not conclusively proving – that they formed from gas that originated outside the bulge. While it is problematic whether or not the young clusters found near the GC formally belong to the bulge, they nevertheless contribute young stars to the inner bulge as they dissolve (Figer et al. 1999). In the case of M31, the absence of bright resolved sources at ultraviolet wavelengths (Bohlin et al. 1985, Brown et al. 1998) indicates that the central regions of this galaxy do not contain the very young stars that are seen near the GC, although the integrated spectrum of the central regions of the M31 bulge shows signatures of an intermediate-age component (Bica et al. 1990; Davidge 1997; Sil'Chenko, Burenkov, & Vlasyuk 1998), which may be the relic of nuclear star forming activity that terminated a few Gyr in the past (Davidge 2001b).

The relative contribution from any young or intermediate-age component to the total light from a bulge might be expected to increase towards later morphological types if, as suggested by Andredakis et al. (1995) and Courteau et al. (1996), interactions with the disk become more significant for these systems. Late-type spiral galaxies are thus important laboratories for assessing interactions between the inner disk and bulge. In the first paper of this series (Davidge 2000; hereafter Paper 1), deep J, H, and Ks images obtained with the Canada-France-Hawaii Telescope (CFHT) Adaptive Optics Bonnette (AOB) were used to investigate the stellar content of the central regions of M33, which is the closest Sc galaxy. These data indicate that the star forming history in the inner disk of M33 during recent epochs has not been continuous. Moreover, the depth of 2.3μm CO absorption in the integrated light of the central light concentration of M33 is consistent with a moderately low metallicity, indicating that it could not have formed from material in the present-day disk. While the low metallicity suggests that the main body of the central light concentration is likely not young, and may even be an inward extension of the halo (Bothun 1992), the nucleus has a near-infrared SED reminiscent of intermediate age Magellanic Cloud clusters and Sgr A (Davidge 2000). Gordon et al. (1999) concluded that the nucleus of M33 contains a significant amount of dust, with a major burst of star formation occuring some 70 Myr in the past.

It remains to be determined if the stellar content in the central regions of M33 is representative of other Sc galaxies. In the present work, the stellar contents in the central regions of the Sc galaxies NGC 247 and NGC 2403 are investigated and compared with M33. These galaxies are close enough that the brightest inner disk stars can be resolved. Moreover, they are viewed at intermediate inclination angles, so that their central light concentrations are likely not heavily obscured by dust in the disk. Finally, gas in the disk of NGC 2403 has a chemical composition that is similar to M33 (Garnett et al. 1997), and

so young and intermediate age stars in these galaxies should have comparable metallicities.

The morphological type, integrated apparent B brightness, total extinction, true distance modulus, and integrated absolute B brightness of M33, NGC 247, and NGC 2403 are listed in Table 1. The extinction estimates are based on the model described by Tully & Fouqué (1985), as applied by Pierce & Tully (1992). The extinction in the disks of spiral galaxies can be patchy and, in the case of NGC 2403, A_V towards H II regions varies between 0.2 – 0.9 mag (McCall, Rybski, & Shields 1985; Petersen & Gammelgaard 1996), which corresponds to E(J–K) ranging from 0.03 mag to 0.15 mag using the Rieke & Lebofsky (1985) extinction curve. Consequently, while the extinction entries in Table 1 likely hold for each system when averaged over large angular scales, they may not reflect the actual values in the inner disk and nucleus, and we estimate the uncertainty in E(J–K) to be ± 0.06 mag based on the extinction measurements towards H II regions in NGC 2403.

The distance moduli of M33 and NGC 2403 in Table 1 are from van den Bergh (1992) and Freedman & Madore (1988), respectively. NGC 247 has by far the most uncertain distance modulus, in large part because there are no published Cepheid observations. The distance modulus listed in Table 1 for this galaxy was derived from the Tully-Fisher relation, using line widths and integrated B, R, and I brightnesses from Pierce & Tully (1992), and the calibrating relations from Sakai et al. (2000). The result agrees within a few tenths of a dex with the distance derived for NGC 253, which is located close to NGC 247 on the sky, using the brightest halo (Davidge & Pritchet 1990) and disk (Davidge, Le Fèvre, & Clark 1991) stars.

The paper is structured as follows. The observations and data reduction procedures are described in §2. The photometric properties of resolved stars in the inner disks of NGC 247 and NGC 2403 are discussed in §3, while the integrated photometric properties of the central light concentrations of these galaxies are compared in §4. Comparisons are made with M33 throughout the paper using the data discussed by Davidge (2000), which have been processed to simulate the appearance of this galaxy if observed at the same distance and with the same angular resolution as NGC 2403. A summary and discussion of the results follows in §5.

2. OBSERVATIONS AND REDUCTIONS

The data were recorded with the CFHT AOB (Rigaut et al. 1998) and KIR imager during observing runs in 1998, 1999, and 2000. The detector in KIR is a 1024×1024 Hg:Cd:Te array, with each pixel subtending $0''.034 \times 0''.034$ on the sky; hence, a 35×35

arcsec region is imaged.

J, H, and Ks images centered on an uncatalogued $K = 10$ star, located 23 arcsec south west of the nucleus of NGC 2403 with α = 07:36:48 and δ = +65:35:41 (E2000), were recorded on the night of UT March 8, 1998. This star was the reference beacon for AO compensation, and is not listed in either the HST or USNO Guide Star catalogues because the central regions of NGC 2403 are overexposed on the POSS. Ten 30 second integrations per filter were recorded at each corner of a $0''.5 \times 0''.5$ square dither pattern, so that the total exposure time was $10 \times 30 \times 4 = 1200$ sec per filter. This same dither pattern was adopted for the other fields discussed in this paper. The FWHMs of stars in the final images of this field are $0''.20$ (J), $0''.15$ (H), and $0''.17$ (Ks). This field will be refered to as the 'deep' NGC 2403 field for the remainder of the paper.

J, H, and Ks images of a second NGC 2403 field, which includes the galaxy nucleus and will be refered to as the 'central' NGC 2403 field, were recorded during the night of UT September 10, 2000. The field center was chosen so that there would be significant overlap with the deep field, and the uncatalogued $K = 10$ star described in the previous paragraph was used as the reference source for AO guiding. Two 60 second exposures per filter were recorded at each dither position, and the total exposure time is thus $2 \times 60 \times 4 = 480$ seconds per filter. The FWHMs of stars in the final images of this field are $0''.17$ (J), $0''.15$ (H), and $0''.19$ (Ks).

J, H, and Ks images of the center of NGC 247 were recorded during the nights of UT June 20 and 21 1999. The NGC 247 line of sight passes near the South Galactic Pole, and there are no stars near the center of this galaxy that are bright enough ($R \leq 15$) to serve as AO guide sources; consequently, the central light concentration of NGC 247 was used as the AO reference source. The NGC 247 data were recorded with 60 second integration times, and the total exposure time was 8 minutes in J, 17 minutes in H, and 20 minutes in Ks. The image quality of these data is poor by AOB standards, as the central light concentration is extended and near the faint limit of the AOB wavefront sensor. The FWHMs of stars in this field are $0''.68$ (J), $0''.54$ (H), and $0''.48$ (Ks).

The data were reduced using the procedures described in Paper 1, which correct for the dark current, pixel-to-pixel sensitivity variations, vignetting along the optical path, the DC sky level, interference fringes, and thermal emission signatures. The processed images were then aligned, median-combined, and trimmed to the area of common overlap for each field. The final Ks images are shown in Figures 1, 2, and 3; the central light concentrations of NGC 247 and NGC 2403 are marked in Figures 2 and 3.

3. PHOTOMETRIC PROPERTIES OF RESOLVED STARS

3.1. Photometric Measurements

A single PSF was constructed for each field using tasks in DAOPHOT (Stetson 1987), and the brightnesses of individual stars were then measured with the PSF-fitting routine ALLSTAR (Stetson & Harris 1988). While anisoplanicity causes the PSF to change with distance from the AO reference star, photometric studies of globular clusters with the AOB indicate that these variations typically introduce scatter of only a few hundredths of a magnitude over the KIR field (e.g. Davidge & Courteau 1999; Davidge 2001a). The unresolved background in each galaxy, which can cause scatter in the photometry if it is non-uniform over angular scales comparable to, or smaller than, that of the sky annulus used by ALLSTAR, was subtracted from each field using the iterative technique described by Davidge et al. (1991).

Artificial star experiments, in which scaled PSFs were added with noise to the images with the DAOPHOT ADDSTAR routine, were used (1) to estimate completeness, (2) to assess the uncertainties introduced by random noise and crowding, and (3) to measure systematic effects in the photometry that cause stars near the faint limit to appear brighter than they actually are. The artificial stars were assigned colors representative of real objects in each field, and were constructed using the PSFs discussed in the preceding paragraph. The artificial star experiments thus assume that anisoplanicity does not significantly affect the photometry, and evidence to support this assumption is given in §3.2.

3.2. Color-Magnitude and Two-Color Diagrams

The $(H, J-H)$, $(K, H-K)$ and $(K, J-K)$ CMDs of stars detected in the NGC 247 and NGC 2403 fields in all three filters are shown in Figures 4, 5, and 6. The PSF wings of the bright AO guide star elevate the sky level in the region immediately surrounding this object; not only does this affect the faint limit, but it also adds noise, which may be mis-identified as stars. To avoid these problems, sources within $4''.25$ of this star were not considered in this study.

The CMDs contain a red plume, the width of which is consistent with the scatter predicted by the artificial star experiments. This indicates that observational errors, rather than intrinsic star-to-star differences in photometric properties, are the dominant source of scatter in the data. The good agreement between the predicted and observed widths of the red plume also indicates that anisoplanicity is not a major contributor to the photometric

errors.

The photometric calibrations of the two NGC 2403 datasets are remarkably consistent, as the mean difference in the K brightness of sources common to both fields is $\Delta K = -0.01 \pm 0.02$, where the difference is in the sense center field minus deep field. The quoted uncertainty is the standard error of the mean. Some of these stars might be variable; however, the modest dispersion in ΔK suggests that the brightest sources common to both fields have typically not varied in K by more than a few hundredths of a magnitude in the 1.5 years separating the observations.

The CMDs in Figures 4 - 6 are dominated by a mixture of red supergiants (RSGs) and stars evolving on the AGB. RSGs are massive stars that burn material in a non-degenerate core, while AGB stars are burning material in a shell around an electron degenerate core (e.g. Iben 1974; Wood, Bessell, & Fox 1983). At solar metallicities the onset of the AGB in simple stellar systems occurs at an age $\log(t_{Gyr}) = 8.1$, which corresponds to stars near 5 $M_{\odot}$ (Girardi et al. 2000).

RSGs and AGB stars have very different near-infrared photometric properties. RSGs in the LMC and SMC define a roughly vertical sequence on the ($M_K, J - K$) CMD, which extends from $M_K = -9$ to $M_K = -12$, whereas long period variables (LPVs), the majority of which are evolving on the AGB, are redder, fainter, and distributed over a broader range of colors (e.g. Figure 8 of Davidge 1998, which was constructed using data from Elias, Frogel, & Humphreys 1985, Wood et al. 1983, and Wood, Bessell, & Paltoglou 1985). RSGs dominate star counts in the LMC and SMC when $M_K < -10$, and so the red stars with $K < 17.5$ in NGC 2403 and $K < 17$ in NGC 247 are likely RSGs. AGB stars dominate in the Magellanic Clouds when $M_K > -9$, which corresponds to $K > 18.5$ in NGC 2403 and $K > 18$ in NGC 247. The tendency for the NGC 2403 CMDs to become redder when $K > 18$ is consistent with the onset of a bright AGB component.

The CMDs of the two NGC 2403 fields also show that a modest blue population, with $K \sim 18$, is present. These stars have $M_K \sim -9.5$, and are too bright to be main sequence OB stars, which have $M_K > -5$ (e.g. Cotera et al. 2000); rather, these stars are likely early-type supergiants. In addition, two of the brightest sources near the center of NGC 2403 are non-stellar, and these objects also appear to be extended in the HST F160W and F187N images of NGC 2403 used by Böker et al. (1999) in their study of the central regions of nearby spiral galaxies. These objects have unremarkable brightnesses in the F187N images, indicating that they have weak or non-existent Paα emission; hence, they are likely not compact H II regions, but could be blends of two or more stars, or possibly even compact star clusters. These objects are marked in Figure 2.

The presence of red and early-type supergiants indicates that star formation occured within the past ~ 0.1 Gyr in the inner disk of NGC 2403. Drissen et al. (1999) conducted an Hα survey of NGC 2403, and an inspection of their Figure 1 indicates that while there is diffuse Hα emission near the center of the galaxy, the surface brightness is markedly lower than in the surrounding areas. Massive stars can deposit significant amounts of energy into the interstellar medium (e.g. Leitherer, Robert, & Drissen 1992), and the resulting winds can produce H II bubbles (e.g. Tarrab 1983). The distribution of Hα emission near the center of NGC 2403 suggests that the recent star-forming event near the center of NGC 2403 may have been sufficiently intense to form such a bubble.

The ($M_K, J-K$) CMDs of NGC 247 and NGC 2403, corrected for interstellar extinction using the entries listed in Table 1 and the Rieke & Lebofsky (1985) reddening law, are shown in Figure 7. Also plotted is a CMD of the central regions of M33. NGC 247 and NGC 2403 are more distant than M33, and this could affect efforts to make comparisons with M33, as blending, which occurs when stars fall within the same resolution element, will be less of a concern for nearby systems. To remove this potential source of systematic error, the M33 data from Paper 1 were processed to simulate the appearance of this galaxy if (1) shifted to the same distance as NGC 2403, and (2) observed with the same angular resolution as the NGC 2403 central field. This was done by block-averaging each M33 image in 4×4 pixel groups, and then smoothing the result with a gaussian to match the FWHM of the NGC 2403 data. The M33 measurements shown in Figure 7 were obtained from the resulting images.

In Paper 1 it was found that the brightest stars near the center of M33 have $M_K \sim -9$, and this is roughly consistent with the CMD in Figure 7. Nevertheless, there is a spray of objects with $M_K \leq -9$ that are likely blends introduced by the simulated increase in distance. The relative number of blended sources in the NGC 2403 data will be smaller than predicted from the M33 data, as only a region that is very close to the central light concentration is sampled in M33, whereas the NGC 2403 data covers a much larger range of distances from the central light concentration, with a corresponding lower mean stellar density.

The red plume of NGC 2403 in Figure 7 peaks near $M_K \sim -11.5$, which is comparable to the peak RSG brightness for galaxies with integrated brightnesses comparable to NGC 2403 (Rozanski & Rowan-Robinson 1994). The brightest source in the two NGC 2403 fields is stellar, although the second and third brightest sources are non-stellar, and hence are not individual stars. The spatial distribution of stars within two magnitudes of the peak K brightness near the center of NGC 2403 (i.e. with $M_K \leq -9.5$) is shown in Figure 8, and it is evident that recent star-forming activity, as traced by these RSGs, has occured mainly to

the South of the nucleus.

The peak brightnesses in NGC 247 and M33 are roughly one magnitude fainter in K than in NGC 2403. Although having similar peak brightnesses, the stellar contents of the central regions of NGC 247 and M33 differ, in that there is a more-or-less continuous population of stars in the interval between $M_K = -9.5$ and -10.5 in the CMD of the former, whereas this brightness interval is poorly populated in the CMD of the latter.

When compared with NGC 2403, the angular resolution of the NGC 247 data are relatively poor, and blending of unresolved stars is a potential concern. The effects of blending were investigated using the F160W NIC3 image (frame N4K416C9Q) of NGC 247 that was obtained as part of the survey of the central regions of nearby late-type galaxies described by Böker et al. (1999). The image was retrieved from the CADC HST archive and pipeline processed; cosmic rays and bad pixels were identified and suppressed by interpolating between surrounding pixels. The processed image was gaussian smoothed to an angular resolution of $0''.6$ to match the CFHT NGC 247 observations. DAOPHOT and ALLSTAR were then used to measure the brightnesses of sources from the smoothed and unsmoothed images, and the difference between these, Δ, was computed. For sources between $H = 17$ and $H = 20$ $\Delta \sim 0$, with a standard deviation ± 0.05 mag. Δ does not depart significantly from 0 until $H \geq 20$, which is well below the faint limit of the CFHT data. Hence, the photometric measurements of bright sources in NGC 247 shown in Figures 4, 5, and 6 are not affected by blending.

M33 is much closer than the other galaxies, and so the KIR field samples an intrinsically smaller portion of this galaxy. This difference in spatial coverage could affect the comparisons in Figure 7 if there is a radial gradient in stellar content, or simply because of small number statistics. Indeed, McLean & Liu (1996) found stars as bright as $M_K = -10.5$ within a few arcmin of the center of M33. If only the portion of NGC 2403 that corresponds to the region sampled in M33 is considered, then the brightest star has $M_K = -10.2$, while the brightest star in the corresponding region of NGC 247 has $M_K = -9.5$. Thus, significant differences in bright stellar content remain even when similar regions of the galaxies are compared.

The $(J - H, H - K)$ two-color diagrams (TCDs) of the stars detected in the central fields of NGC 247 and NGC 2403 are shown in Figure 9, along with fiducial sequences defined by Milky-Way RSGs and LPVs in the LMC and SMC. Aside from a modest clump of early-type supergiants with $H - K = J - H = 0$ in the NGC 2403 TCD, the data for both galaxies match the RSG and LPV fiducial sequences. There is an absence of extremely red LPVs in the upper right hand corner of the TCD. These stars tend to have $M_K \geq -8.5$, and hence are too faint to be detected with the current data.

3.3. Luminosity Functions

The completeness-corrected M_K luminosity functions (LFs) of stars detected in both H and K in NGC 2403 and M33 are compared in Figure 10. The LF for NGC 2403 was constructed by combining the LFs of the central and deep fields, such that the entries for $M_K > -10$ are from the deep field after scaling to match the number of stars in the central field with $M_K < -10$, while those for brighter stars are from the central field. The resulting composite LF was then scaled to match the mean surface brightness in the M33 field using the $r-$band surface brightness profiles for M33 and NGC 2403 measured by Kent (1987a,b). Despite the differences in stellar content evident when $M_K \leq -9.5$ in Figure 7, the LFs of M33 and NGC 2403 agree within their estimated uncertainties between $M_K = -9.5$ and $M_K = -8$, which is a brightness interval dominated by luminous AGB stars. Thus, the star-forming histories of the innermost disks of NGC 2403 and M33 have been similar on ~ 1 Gyr time scales.

4. NUCLEAR PROPERTIES

In §3 it was demonstrated that the recent ($t \leq 1$ Gyr) star forming histories of the inner disks of NGC 247, NGC 2403, and M33 have been different. If star forming episodes in the nuclei and inner disks of late-type spiral galaxies are somehow related (e.g. they are triggered by the same mechanism), then the nuclear photometric properties of NGC 247, NGC 2403, and M33 ought to show significant differences as well. The nuclear photometric properties of these galaxies are investigated in this section.

4.1. Color Profiles

The colors of the central light concentrations of NGC 247 and NGC 2403 were measured in a series of concentric circular apertures, and the results are plotted in Figures 11 (integrated measurements) and 12 (differential measurements). The minimum aperture diameter for NGC 2403 was set at $0\farcs25$, and this was increased in $0\farcs25$ increments. A coarser sampling was used for NGC 247 because of the poorer angular resolution of these data: the minimum aperture diameter was $0\farcs5$, and this was increased in $0\farcs5$ increments. The measurements, which were restricted to a maximum radius of $1\farcs25$, were made after the H and K data for each galaxy had been smoothed to match the angular resolution of the J data, which had the poorest angular resolution in each dataset. The local background was measured in an annulus immediately surrounding each central light

concentration to minimize contamination from the inner disk. A corresponding set of aperture measurements were made from the M33 data from Paper 1 after these were block-averaged and gaussian-smoothed to match the distance and angular resolutions of the NGC 247 and NGC 2403 data.

While the means exist to perform a more complicated photometric analysis of the central regions of these galaxies with finer angular sampling, it was decided not to pursue these because anisoplanicity introduces subtle non-uniformities in the PSF, which could have a major impact on photometric measurements made on angular scales less than the FWHM. Rather, it was felt that aperture measurements with angular scales comparable to the FWHM of the images would provide a more robust means of comparing the central photometric properties of these galaxies.

The colors measured for NGC 247 are broadly consistent with those published by Frogel (1985), who found that $J - K = 0.75$ and $H - K = 0.14$ through a $6''.3$ aperture; for comparison, the current data give $J - K = 0.68$ and $H - K = 0.13$ through a $1''.0$ radius aperture. Given that the uncertainty in the current colors due to the photometric calibration is ± 0.04 mag, then the agreement with the Frogel (1985) measurements is good.

Pierini et al. (1997) measured $H - K = 0.17$ within $1''.6$ of the center of NGC 2403, and $H - K = 0.14$ within $4''.8$, while the present data give $H - K = 0.04$ mag within a $1''.25$ radius. We have confidence in the photometric calibration of our NGC 2403 data because (1) the locus of resolved stars on the CMDs of M33 and NGC 2403 in Figure 7 have similar colors, even though the integrated colors of the central light concentrations differ at roughly the 5σ level, and (2) when placed on the near-infrared TCD, stars in NGC 2403 fall along fiducial sequences (Figure 9), which would not be the case if the photometric calibration were greatly in error.

The colors in Figures 11 and 12 were also checked using 2MASS images of NGC 247 and M33; unfortunately, the NGC 2403 data could not be checked in this way since this portion of the 2MASS survey has not yet been released. The 2MASS images of NGC 247 give a color of $J - K = 0.66$ within 1 arcsec of the galaxy center, which is in excellent agreement with what is measured here. The 2MASS data also indicate that $J - K$ becomes bluer with increasing radius in NGC 247, in qualitative agreement with the color profiles in Figures 11 and 12. As for M33, the 2MASS images confirm the relatively red central color of this galaxy, although they give $J - K = 0.90$ within the central $1''.0$ of this galaxy, whereas the current data give $J - K = 0.81$. The 2MASS data also indicate that $J - K$ increases towards larger radius in M33, in qualitative agreement with the trends in Figures 11 and 12.

It is evident from Figures 11 and 12 that (1) the nuclear $J-K$ color of NGC 2403 is bluer than M33, and (2) the central light concentration of NGC 2403 contains a marked color gradient, similar in amplitude to that in M33. Given the qualitatively similar radial color gradients in the central light concentrations of M33 and NGC 2403, and that the former contains a young nuclear star cluster (Gordon et al. 1999; Paper 1), then a young nuclear component is likely also present in the latter. NGC 2403 contains the bluest nuclear population of the three galaxies considered here, while the resolved stellar content within 20 arcsec of the nucleus indicates that the inner disk of this galaxy has experienced the most recent star-forming activity. This consistency in the relative ages of the nucleus and inner disk hints that the star-forming histories of these components may have been coupled.

The $J-K$ colors of NGC 247 and M33 do not differ significantly when $r \leq 0''.5$, suggesting that these galaxies have similar nuclear stellar contents. It is interesting that the $J-K$ gradient near the center of NGC 247 is in the opposite sense to the gradients in M33 and NGC 2403. Nevertheless, the near-infrared SED changes with radius in a way that is still consistent with an increase in the number of younger stars towards smaller radii (see below).

The extinction in the nucleus is a significant source of uncertainty when interpreting Figures 11 and 12. Gordon et al. (1999) find that $A_V \sim 1.4$ mag ($\tau_V = 1.3$) in the nucleus of M33, which corresponds to E(J–K) = 0.23 using the Rieke & Lebofsky (1985) reddening law. For comparison, the extinction listed for M33 in Table 1, which was adopted for Figures 11 and 12, gives E(J–K) = 0.04 mag. The effect of adopting the higher extinction for the nucleus of M33 is shown in Figures 11 and 12, and it is evident that the nuclei of M33 and NGC 2403 may have similar intrinsic colors if they are subject to different amounts of extinction, in the sense that M33 is very dusty and NGC 2403 is relatively dust-free.

The $(J-H, H-K)$ TCD provides a quantitative means of comparing the near-infrared SEDs of the centers of these galaxies. Luminosity-weighted $J-H$ and $H-K$ colors were calculated for each galaxy in the radial intervals $r \leq 0''.5$ and $0''.5 \leq r \leq 1''.25$, and the near-infrared TCDs of the results are shown in Figure 13. The NGC 247 and NGC 2403 data were de-reddened using the A_B entries in Table 1; however, to demonstrate the effects of extinction on the interpretation of the TCD, the M33 data were de-reddened using both the A_B entry for this galaxy in Table 1, and the extinction estimated by Gordon et al. (1999), and so the TCDs in Figure 13 show two points for M33. Also plotted in Figure 13 are (1) the colors of Galactic globular clusters from Table 5A of Brodie & Huchra (1990), (2) the colors of confirmed SWB type 1 and 2 Magellanic Cloud clusters, which are among the youngest clusters in the Magellanic Clouds (e.g. Hodge 1983), from Tables 4 and 5 of Persson et al. (1983), (3) the $6''.6$ aperture measurements of the nuclei of nearby Sc galaxies

from Table 4 of Frogel (1985), and (4) the effects of varying age from 1.5 to 3.0 Gyr for a solar metallicity population (top panel), and of varying the metallicity of a 1.5 Gyr population from solar to [Fe/H] = -0.22 and $+0.25$ (lower panel), as predicted from the models computed by Worthey (1994). Frogel (1985) did not correct for extinction internal to the galaxies, and his data in Figure 13 have been corrected for extinction within each disk by assuming that $E(B-V) = 0.09$, as predicted by Tully & Fouqué (1985) for disk galaxies with an inclination angle of 45°.

The luminosity-weighted colors in the two radial intervals of each galaxy define significantly different locations on the TCD, as expected if there are population gradients near the centers of these galaxies. Moreover, it is evident from the M33 datapoints in Figure 13 that the effects of extinction can be significant. Nevertheless, broad conclusions can still be drawn from the TCD.

NGC 247 and M33 have comparable locations on the TCD when $r \leq 0''.5$, and this is consistent with these systems having similar $J-K$ colors in Figures 11 and 12. The innermost regions of NGC 247 and M33 occupy the same area of the near-infrared TCD as SWB Type 1 and 2 clusters in the Magellanic Clouds, and this holds for the two A_V values considered for M33. The data thus indicate that the nuclei of these galaxies are dominated by intermediate age populations. It is also evident from the top panel of Figure 13 that the nucleus of NGC 2403 has a near-infrared SED that is very different from the nuclei of the other galaxies. The Worthey (1994) models suggest that the location of the nucleus of NGC 2403 on the near-infrared TCD can not easily be explained with respect to NGC 247 and M33 simply by involking differences in age and/or metallicity. However, Worthey (1994) did not model systems with $t \leq 1.5$ Gyr, and the trends defined by the models shown in Figure 13 may not hold for significantly younger populations.

The circumnuclear regions of the three galaxies also show a broad range of near-infrared photometric properties. The NGC 247 and NGC 2403 measurements when $r \geq 0''.5$ are located in the same region of the near-infrared TCD as Galactic globular clusters; hence, the circumnuclear regions of these galaxies have near-infrared photometric properties that are consistent with them being old stellar systems. In addition, even though NGC 247 has a color gradient that is in the opposite sense to that in the other 2 systems, the near-infrared SED is still consistent with a radial gradient in mean age, in the sense of younger stars occuring at smaller radii.

4.2. K–Band Surface Brightness Profiles

The $K-$band surface brightness profiles of the central regions of NGC 247, NGC 2403, and M33, obtained from the aperture measurements discussed in §4.2, are compared in Figure 14. After adjusting for differences in seeing and distance, the mean $K-$band surface brightnesses near the centers of NGC 247 and NGC 2403 are $1 - 2$ mag arcsec^{-2} fainter than in M33. This difference in surface brightness is not due to uncertainties in the image quality, as experiments indicate that even if the image quality of the M33 data were increased by $0''.1$ with respect to the other systems then the mean surface brightness of M33 within the central aperture is lowered by only ~ 0.1 mag arcsec^{-2}. The surface brightnesses are also not sensitive to extinction, as adopting the higher extinction for the M33 nucleus proposed by Gordon et al. (1999) changes the $K-$band surface brightness near the center of this galaxy by only 0.1 mag, and this is in the sense of making the nucleus even brighter. Hence, when comparing mean surface brightnesses within a given aperture, M33 has an intrinsically higher $K-$band surface brightness than within $0''.12$ of the center of NGC 2403, and within $0''.25$ of the center of NGC 247.

The extreme compact nature of the M33 nucleus has long been recognized (e.g. Kormendy & McLure 1993). We suggest that the high central surface brightness may not be due exclusively to a high mass concentration, but could be, at least in part, a result of stellar content effects. The nucleus of M33 has a relatively strong central CO index (Paper 1), suggesting that there is a centrally concentrated population of red stars, which would elevate the $K-$band surface brightness. High angular-resolution narrow-band CO images do not yet exist for NGC 247 and NGC 2403, but if future observations reveal that the nuclei of NGC 247 and 2403 have weaker CO indices than M33 then stellar content will have to be considered when comparing the central near-infrared surface brightnesses of these galaxies. Based on the $J-K$ colors in Figures 11 and 12 it might be anticipated that the central CO indices of NGC 247 and M33 are similar.

5. DISCUSSION & SUMMARY

JHK images obtained with the CFHT AOB have been used to investigate the stellar contents in the central 30 arcsec of the nearby Sc galaxies NGC 247 and NGC 2403. Stars as faint as $M_K = -8.5$ are detected in the inner disks of both systems. The majority of the resolved stars are RSGs or are evolving on the AGB, although early-type supergiants have also been detected near the center of NGC 2403.

M33, NGC 247, and NGC 2403 were included in the broad and narrow-band NICMOS

imaging survey of late-type systems discussed by Böker et al. (1999), and their data identified isolated ('I') or diffuse nebulosity ('DN') in the 51×51 arcsec NICMOS3 field of view of each system, indicating that recent star formation has occured in the inner disks of these galaxies. Our data, which probe a broader range of ages than is possible with emission line information, reveal that there have been significant galaxy-to-galaxy variations in the recent star forming histories near the centers of these galaxies.

Stochastic variations in the recent star-forming histories of fields within a galaxy are to be expected, and Davidge (1998) found significant galaxy-to-galaxy variations in the infrared-bright stellar content of the late-type Sculptor spiral galaxies NGC 55, NGC 300, and NGC 7793. It might be anticipated that such variations in local star-forming history will diminish as stars sampling progressively longer time intervals are included in the analysis, and the comparison of the K LFs of upper AGB stars in the inner disks of these galaxies in Figure 10 indicates that the star-forming histories of the inner disks of M33 and NGC 2403 have been similar when averaged over Gyr timescales.

Bell & de Jong (2000) used optical and near-infrared photometry to investigate the stellar contents of nearby galaxies, and concluded that disk evolution is driven largely by local mass density. This can be explained if the star-forming history depends on the local gas surface density, as originally proposed by Schmidt (1959). Given that (1) M33 and NGC 2403 are located in relatively uncrowded environments, and hence have likely evolved in relative isolation, and (2) the inner disks of these galaxies have very similar surface brightnesses (Kent 1987a, b), then the Bell & de Jong (2000) results predict that they would have had similar star forming histories, which is consistent with the comparison in Figure 10.

We also compared the integrated near-infrared photometric properties of the central regions of NGC 247 and NGC 2403 with those of M33. Böker et al. (1999) found that NGC 247, NGC 2403, and M33 lack measureable nuclear Paα emission, suggesting an absence of significant nuclear star-forming activity during the last $10 - 100$ Myr. An absence of line emission could occur in the presence of a young population if the ISM has been lost due to winds. However, this can not be the case in M33, as the central regions of this galaxy contain dust (Gordon et al. 1999), indicating that an ISM is present.

There is a $J - K$ color gradient within 1 arcsec of the nucleus of NGC 2403, which is in the same sense as that in the corresponding region of M33. Given that M33 contains a young or intermediate-age nuclear population (Gordon et al. 1999; Paper 1), which causes a color gradient near the center of that galaxy, it is reasonable to conclude that the nucleus of NGC 2403 also contains a young population. The nuclei of NGC 2403 and M33 may have different ages, as the nucleus of NGC 2403 has a bluer $J - K$ color than M33, although

this conclusion assumes that the nuclear dust contents of these systems are similar. The near-infrared SED of the central light concentration surrounding the nucleus of NGC 2403 is consistent with it being an old simple stellar system, at least as defined by Galactic globular clusters. Spectroscopic observations will be necessary to determine if the central light concentrations of M33 and NGC 2403 have similar metallicities and ages.

Drissen et al. (2000) used WFPC2 images to investigate the central regions of NGC 2403, and measured a half light radius of 3.4 parsecs, or $0\farcs22$, for the nucleus. Based on the measured color ($B - V = 0.78$), and the absence of radio (Turner & Ho 1994) and Hα emission, Drissen et al. suggest that the central light concentration of NGC 2403 is old. With an integrated color of $J - K = 0.6$ at $0\farcs5$ radius the current data also indicate that the central regions of this galaxy have a color that is superficially consistent with an old population. However, the color profile clearly indicates that there is a distinct nucleus that is bluer than the surroundings; hence, the central regions of NGC 2403 are not uniformly old.

A color gradient is also seen in the central regions of NGC 247, although it is in the opposite sense to that in NGC 2403 and M33. The $J - K$ color within the central $0\farcs5$ of NGC 247 is similar to that in M33, suggesting that the nuclear stellar contents of NGC 247 and M33 are similar, although this should be confirmed with observations of NGC 247 at higher angular resolutions. While the central light concentration of NGC 247 is bluer than the nucleus, it still has an SED that is consistent with an old simple stellar population.

It is remarkable that the central regions of four of the nearest galaxies of morphological type Sbc (the Milky-Way) and Sc (M33, NGC 247, and NGC 2403) contain relatively young nuclear star clusters. It is also worth noting that the two nearest Sb systems, M31 and M81, show evidence for a young or intermediate-age nuclear population (Davidge 1997, Sil'Chenko et al. 1998, Davidge & Courteau 1999) and/or nuclear activity (Filippenko & Sargent 1988; Davidge & Courteau 1999), although the nuclear population in M31 is older than what is seen near the centers of the Milky-Way and nearby Sc galaxies (Davidge 2001b). The high frequency of young nuclear populations among the closest galaxies is consistent with surveys of more distant systems. Of the 45 unbarred spirals with morphological types Sb and later observed by Böker et al. (1999), 17 show nuclear Paα emission. Ho, Filippenko, & Sargent find an even higher incidence of line emission from star formation in late-type spirals, although their data have a typical spatial resolution of 200×400 parsecs, and so some of this emission undoubtedly originates from the inner disk rather than the nucleus.

Unless one is willing to accept that the central regions of nearby late-type spiral galaxies are being observed at fortuitously similar stages of a once-in-a-galaxy-lifetime occurence, then it appears that nuclear star formation is an episodic or continuous

phenomenon in 'normal' spiral galaxies, with a maximum time between star-forming events such that the nucleus can be easily detected with respect to the surroundings. An estimate for the time scale between significant nuclear star forming events can be obtained from the Böker et al. (1999) survey if it is assumed that the Paα emission is due to star formation, which is reasonable given that AGN and LINER emission tends to occur in galaxies earlier than type Sbc (Ho et al. 1997). If line emission can be detected for ~ 0.1 Gyr after a burst of star formation, then the time between star-forming episodes is 0.1 Gyr $\times 45/17 \sim 0.3$ Gyr.

Serabyn & Morris (1996) discuss mechanisms by which gas from the Galactic disk can be funneled into the central molecular zone (CMZ), which in turn fuels star formation in the central regions of the Galaxy. Observational support of a disk origin for the star-forming material near the GC comes from the flattened nature of the CMZ, which also lies along the Galactic Plane (Bally et al. 1988), and abundance studies of young stars near the GC (Ramirez et al. 2000), although these measurements are restricted at present to Fe lines, and the chemical mixtures in these stars, which will provide a signature of the origin of the material from which they formed, remain to be determined. Serabyn & Morris (1996) argue that the central cusp in the Galactic bulge is sustained by either continuous or frequent bursts of star formation, and they note that a key test of this hypothesis is to determine whether young or intermediate-age nuclear populations are present in other galaxies. *The current data indicate that recent nuclear star formation in nearby galaxies is a common phenomenon, thus supporting the Serabyn & Morris (1996) model of frequent or continuous central star formation.* We note further that the $J - K$ color of the NGC 2403 nucleus suggests that it is younger than the nuclei in the other Sc galaxies if the central extinctions in these systems are similar, and this is consistent with the relative ages of the inner disks, as infered from the resolved bright stellar content. While a larger sample of systems must be observed to establish a rigorous correlation, this is a tantalizing hint that star formation in the nucleus and inner disk might have common triggers.

Is nuclear star formation affected by, or related to, the presence of a super-massive central object? A connection might be expected since super-massive objects affect the central structural characteristics of galaxies (e.g. Faber et al. 1997), and impose demanding constraints on the conditions required to form stars near galaxy centers (e.g. Figer et al. 2000). Indeed, the correlation between the masses of super-massive objects and the velocity dispersion of their host bulges (Ferrarese & Merritt 2000; Gebhardt et al. 2000) suggests that the formation and evolution of the central black hole and bulge are coupled (e.g. Haehnelt & Kauffmann 2000). Nevertheless, Salucci et al. (2000) find that late-type spiral galaxies may not fall along the relation between black hole mass and bulge mass defined by early-type spirals and ellipticals, in the sense that the central objects in late-type galaxies

are less massive than those in early-type galaxies having the same bulge mass. This could be a signature of morphology-related systematic differences in the evolutionary histories of bulges, and may explain the tendency for AGN to be found in early-type spirals (e.g. Ho et al. 1987). In any event, while the nuclei of M33 and the Galaxy have similar stellar contents (Paper 1), the GC contains a central compact object (Ghez et al. 1998), which is much more massive than that in M33 (e.g. Kormendy & McClure 1993; Lauer et al. 1998). Thus, it appears that an extremely massive central object is not essential to trigger nuclear star formation, at least among intermediate and late-type spiral galaxies; rather, the results in this paper suggest that nuclear star formation in these systems is driven by non-local factors that also encompass the inner disk.

It is a pleasure to thank an anonymous referee for comments that helped improve the paper.

Galaxy	Type[a]	B_T[b]	A_B[c]	μ_0[d]	M_B
NGC 247	Sc(s)III-IV	9.74	0.46	27.3	–18.0
NGC 2403	Sc(s)III	8.74	0.34	27.5	–19.1
M33	Sc(s)II-III	6.31	0.32	24.5	–18.5

Table 1: Galaxy Properties

[a] From Sandage & Tammann (1987)

[b] From Table 1 of Pierce & Tully (1992)

[c] Sum of Internal and Galactic extinction from Pierce & Tully (1992)

[d] The distance moduli for NGC 2403 and M33 are based on Cepheids, using results from Freedman & Madore (1988) and van den Bergh (1992). Lacking published observations of Cepheids in NGC 247, the distance modulus for this galaxy is based on the Tully-Fisher relation using integrated brightnesses and HI line widths from Pierce & Tully (1992), and the calibration of Sakai et al. (2000).

REFERENCES

Abraham, R. G., Ellis, R. S., Fabian, A. C., Tanvir, N. R., & Glazebrook, K. 1999, MNRAS, 303, 641

Aguerri, J. A. L., Balcells, M., & Peletier, R. F. 2001, A&A, 367, 428

Andredakis, Y., Peletier, R. F., & Balcells, M. 1995, MNRAS, 275, 874

Bally, J., Stark, A. A., Wilson, R. W., & Henkel, C. 1988, ApJ, 324, 223

Barnes, J. E., & Hernquist, L. E. 1992, ARA&A, 30, 705

Bell, E. F., & de Jong, R. S. 2000, MNRAS, 312, 497

Bica, E., Alloin, D., & Schmidt, A. A. 1990, A&A, 228, 23

Binney, J., Dehnen, W., & Bertelli, G. 2000, MNRAS, 318, 658

Blanco, V. M., & Terndrup, D. M. 1989, AJ, 98, 843

Blitz, L., & Spergel, D. N. 1991, ApJ, 379, 631

Bohlin, R. C., Cornett, R. H., Hill, J. K., Hill, R. S., O'Connell, R. W., & Stecher, T. P. 1985, ApJ, 298, 37

Böker, T. et al. 1999, ApJS, 124, 95

Bothun, G. 1992, AJ, 103, 104

Brown, T. M., Ferguson, H. C., Stanford, S. A., & Deharveng, J-M 1998, ApJ, 504, 113

Carollo, C. M. 1999, ApJ, 523, 566

Carollo, C. M., Stiavelli, M., & Mack, J. 1998, AJ, 116, 68

Chaboyer, B., Sarajedini, A., Armandroff, T. E. 2000, AJ, 120, 3102

Cotera, A. S., Erickson, E. F., Colgan, S. W. J., Simpson, J. P., Allen, D. A., & Burton, M. G. 1996, ApJ, 461, 750

Cotera, A. S., Simpson, J. P., Erickson, E. F., Colgan, S. W. J., Burton, M. G., & Allen, D. A. 2000, ApJS, 129, 123

Courteau, S. 1997, in Morphology and Dust Content in Spiral Galaxies, eds D. Block & M. Greenberg (Kluwer: Dordrecht), 255

Courteau, S., de Jong, R. S., & Broeils, A. H. 1996, ApJ, 457, L73

Davidge, T. J. 1997, AJ, 113, 985

Davidge, T. J. 1998, ApJ, 497, 650

Davidge, T. J. 2000, AJ, 119, 748 (Paper 1)

Davidge, T. J. 2001a, AJ, 121, 3100

Davidge, T. J. 2001b, AJ, 122, 1386

Davidge, T. J., & Courteau, S. 1999, AJ, 117, 1297

Davidge, T. J., & Courteau, S. 1999, AJ, 117, 2781

Davidge, T. J., & Pritchet, C. J. 1990, AJ, 100, 102

Davidge, T. J., Le Fèvre, O., & Clark, C. C. 1991, ApJ, 370, 559

Drissen, L., Roy, J-R, Moffat, A. F. J., & Shara, M. M. 1999, AJ, 117, 1249

Dwek, E. et al. 1995, ApJ, 445, 716

Elias, J. H., Frogel, J. A., & Humphreys, R. M. 1985, ApJS, 57, 91

Faber, S. M. et al. 1997, AJ, 114, 1771

Feltzing, S., & Gilmore, G. 2000, A&A, 355, 949

Ferrarese, L., & Merritt, D. 2000, ApJ, 539, L9

Figer, D. F., Kim, S. S., Morris, M., Serabyn, E., Rich, R. M., & McLean, I. S. 1999, ApJ, 525, 750

Figer, D. F. et al. 2000, ApJ, 533, L49

Filippenko, A. V., & Sargent, W. L. W. 1988, ApJ, 324, 134

Freedman, W. L., & Madore, B. F. 1988, ApJ, 332, L63

Friedli, D., & Benz, W. 1993, A&A, 268, 65

Friedli, D., & Benz, W. 1995, A&A, 309, 649

Frogel, J. A. 1985, ApJ, 298, 528

Frogel, J. A., Persson, S. E., & Cohen, J. G. 1980, ApJ, 240, 785

Garnett, D. R., Shields, G. A., Skillman, E. D., Sagan, S. P., & Dufour, R. J. 1997, ApJ, 489, 63

Gephardt, K. et al. 2000, ApJ, 539, L13

Ghez, A. M., Klein, B. L., Morris, M., & Becklin, E. E. 1998, ApJ, 509, 678

Girardi, L., Bressan, A., Bertelli, G., & Chiosi, C. 2000, A&AS, 141, 371

Gneden, N. Y., Norman, M. L., & Ostriker, J. P. 2000, ApJ, 540, 32

Gordon, K. D., Hanson, M. M., Clayton, G. C., Rieke, G. H., & Misselt, K. A. 1999, ApJ, 519, 165

Haehnelt, M. G., & Kauffmann, G. 2000, MNRAS, 318, L35

Harris, W. E., Harris, G. L. H., & McLaughlin, D. E. 1998, AJ, 115, 1801

Ho, L. C., Filippenko, A. V., & Sargent, W. L. W. 1997, ApJ, 487, 568

Hodge, P. W. 1983, ApJ, 264, 470

Iben, I. Jr. 1974, ARAA, 12, 215

Katz, N. 1992, ApJ, 391, 502

Kent, S. M. 1992, ApJ, 387, 181

Kent, S. M. 1987a, AJ, 93, 816

Kent, S. M. 1987b, AJ, 94, 306

Kong, X. et al. 2000, AJ, 119, 2745

Kormendy, J., & McClure, R. D. 1993, AJ, 105, 1793

Lauer, T. R., Faber, S. M., Ajhar, E. A., Grillmair, C. J., & Scowen, P. A. AJ, 116, 2263

Leitherer, C., Robert, C., & Drissen, L. 1992, ApJ, 401, 596

MacArthur, L., Courteau, S., & Holtzman, J. 2002, in preparation

McCall, M. L., Rybski, P. M., & Shields, G. A. 1985, ApJS, 57, 1

McLean, I. S., & Liu, T. 1996, AJ, 456, 499

Mighell, K. J., & Rich, R. M. 1995, AJ, 110, 1649

Mihos, J. C., & Hernquist, L. E. 1996, ApJ, 464, 641

Minniti, D. 1995, AJ, 109, 1663

Mollá, M., Ferrini, F., & Gozzi, G. 2000, MNRAS, 316, 345

Noguchi, M. 1999, ApJ, 514, 77

Noguchi, M. 2000, MNRAS, 312, 194

Ortolani, S. et al. 1995, Nature, 377, 701

Peletier, R. F., Balcells, M., Davies, R. L., Andredakis, Y., Vazdekis, A., Burkert, A., & Prada, F. 1999, MNRAS, 310, 703

Persson, S. E., Aaronson, M., Cohen, J. G., Frogel, J. A., & Matthews, K. 1983, ApJ, 266, 105

Petersen, L., & Gammelgaard, P. 1996, A&A, 308, 49

Phillips, A. C., Illingworth, G. D., MacKenty, J. W., & Franx, M. 1996, AJ, 111, 1566

Pierce, M. J., & Tully, R. B. 1992, ApJ, 387, 47

Pierini, D., Gavazzi, G., Boselli, A., & Tuffs, R. 1997, A&AS, 125, 293

Ramirez, S. V., Sellgren, K., Carr, J. S., Balachandran, S. C., Blum, R., Terndrup, D., & Steed, A. 2000, ApJ, 537, 205

Rieke, G. H., & Lebofsky, M. J. 1985, ApJ, 288, 618

Rigaut, F. et al. 1998, PASP, 110, 152

Rosenberg, A., Saviane, I., Piotto, G., & Aparicio, A. 1999, AJ, 118, 2306

Rozanski, R., & Rowan-Robinson, M. 1994, MNRAS, 271, 530

Sakai, S. et al. 2000, ApJ, 529, 698

Salucci, P., Ratnam, C., Monaco, P., & Danese, L. 2000, MNRAS, 317, 488

Sandage, A., & Tammann, G. A. 1987, A Revised Shapley-Ames Catalog of Bright Galaxies (Second Edition), Carnegie Institution of Washington.

Sellwood, J. A., & Moore, E. M. 1999, ApJ, 510, 125

Serabyn, E., & Morris, M. 1996, Nature, 382, 602

Schmidt, M. 1959, ApJ, 129, 243

Sil'Chenko, O. K., Burenkov, A. N., & Vlasyuk, V. V. 1998, A&A, 337, 349

Steinmetz, M., & Mueller, E. 1994, A&A, 281, L97

Stetson, P. B. 1987, PASP, 99, 191

Stetson, P. B., & Harris, W. E. 1988, AJ, 96, 909

Tarrab, I. 1983, A&A, 125, 308

Tully, R. B., & Fouqué, P. 1985, ApJS, 58, 67

Turner, J. L., & Ho, P. T. P. 1994, ApJ, 421, 122

van den Bergh, S. 1992, PASP, 104, 861

Wood, P. R., Bessell, M. S., & Fox, M. W. 1983, ApJ, 272, 99

Wood, P. R., Bessell, M. S., & Paltoglou, G. 1985, ApJ, 290, 477

Worthey, G. 1992, ApJS, 95, 107

FIGURE CAPTIONS

Fig. 1.— The final Ks image of the NGC 2403 deep field. The image covers 34×34 arcsec with North at the top and East to the left. The bright central source is the uncatalogued $K = 10$ star with α = 07:36:48 and δ = +65:35:41 (E2000) that was used as the AO guide star.

Fig. 2.— The final Ks image of the NGC 2403 central field. The image covers 34×34 arcsec with North at the top and East to the left. The bright source in the lower right hand corner is the uncatalogued $K = 10$ star that was used as the AO reference beacon, and defines the center of the NGC 2403 deep field in Figure 1. The central light concentration of NGC 2403 is circled, while squares mark the two extended objects discussed in §3.2.

Fig. 3.— The final Ks image of the NGC 247 central field. The image covers 34×34 arcsec with North at the top and East to the left. The central light concentration of NGC 247, which served as the reference source for AO guiding, is circled.

Fig. 4.— The $(H, J - H)$ CMDs of stars in the NGC 2403 and NGC 247 fields that were detected in all 3 filters. The error bars show the 1σ uncertainties predicted from artificial star experiments. The predicted uncertainties match the observed width of the red plume in each galaxy, indicating that the scatter in the CMDs is dominated by observational errors. The stars with $J - H = 0$ in both NGC 2403 fields are likely early-type supergiants.

Fig. 5.— The $(K, H - K)$ CMDs of stars in the NGC 2403 and NGC 247 fields that were detected in all 3 filters. The error bars show the 1σ uncertainties predicted from artificial star experiments. The predicted uncertainties generally match the width of the red plume in each galaxy, indicating that the scatter in the CMDs is dominated by observational errors.

Fig. 6.— The $(K, J - K)$ CMDs of stars in the NGC 2403 and NGC 247 fields that were detected in all 3 filters. The error bars show the 1σ uncertainties predicted from artificial star experiments. The predicted uncertainties match the width of the red plume in each galaxy, indicating that the scatter in the CMDs is dominated by observational errors. The stars with $J - K = 0$ in both NGC 2403 fields are early-type supergiants.

Fig. 7.— The $(M_K, J - K)$ CMDs of the NGC 2403 deep field, the central fields of NGC 2403 and NGC 247, and the central regions of M33. The M33 CMD was obtained from the data discussed in Paper 1, after these were processed to simulate moving this galaxy to the distance of NGC 2403 and then observing with the same angular resolution as the NGC 2403 central field. The filled squares in the NGC 2403 central field CMD mark sources that are non-stellar in appearance. The adopted distance moduli and extinctions for each field are

shown. Note the conspicuous differences in the bright stellar contents of the three galaxies.

Fig. 8.— The spatial distribution of RSGs within two magnitudes of the peak K brightness in the NGC 2403 central field. Stars with M_K between -9.5 and -10.5 are plotted as crosses, while stars with $M_K \leq -10.5$ are shown as filled squares. X and Y are offsets, in arcsec, from the center of NGC 2403, with North at the top, and East to the left. Note that the vast majority of these bright stars are located to the South of the nucleus.

Fig. 9.— The $(J-H, H-K)$ two color diagrams of stars in the NGC 2403 and NGC 247 central fields. The dashed line is the locus of LPVs in the LMC and SMC, defined from observations published by Wood et al. (1983, 1985), while the solid line is the locus of Milky-Way RSGs, established from data published by Elias et al. (1985).

Fig. 10.— The completeness-corrected M_K LFs of stars near the centers of NGC 2403 (solid line) and M33 (dashed line), where $n_{0.5}$ is the number of stars per 0.5 mag interval per kpc^2. The error bars show uncertainties due to counting statistics and completeness corrections. The NGC 2403 LF, which was constructed by combining data in the deep and central fields using the procedure described in the text, has been scaled to match the $r-$band surface brightness in the M33 field using the light profiles measured by Kent (1987a, b). The LFs of NGC 2403 and M33 are in excellent agreement between $M_K = -9.5$ and -8.0, indicating that the star-forming histories of the inner disks of these galaxies have been similar over time scales probed by bright AGB stars (~ 1 Gyr).

Fig. 11.— The integrated $J-K$ color profiles of NGC 2403 and NGC 247. The dashed lines show the corresponding color curves for M33 measured from data processed to simulate the appearance of the central field of this galaxy if viewed at the same distance and with the same angular resolution as NGC 2403 and NGC 247. The bluest nuclear $J-K$ color occurs in NGC 2403, and the reddest is in M33; this is broadly consistent with the age sequence predicted from the brightest red stars in the inner disks of these galaxies. The 1σ error bar showing the uncertainty in the photometric calibration, which is the dominant source of random error in the integrated color measurements, is also shown. The arrow shows the result of adopting $A_V = 1.4$ mag for the nucleus of M33, as measured by Gordon et al. (1999). Note that the M33 and NGC 2403 curves in the upper panel differ at roughly the 5σ level if these systems have similar amounts of extinction in their central regions. However, if the extinction in the nucleus of NGC 2403 is significantly less than that in M33 then the nuclei of these galaxies may have similar intrinsic colors.

Fig. 12.— The $J-K$ colors measured in concentric circular annuli for NGC 2403 and NGC 247. The dashed lines show the corresponding color curves for M33 measured from data processed to simulate the appearance of the central field of this galaxy if viewed at

the same distance and with the same angular resolution as NGC 2403 and NGC 247. The bluest nuclear $J-K$ color occurs in NGC 2403, while the reddest is in M33; this is broadly consistent with the age sequence infered from bright red stars in the inner disks of these galaxies. The error bars on the end points of the NGC 2403 and NGC 247 curves show the 1σ uncertainties due to photon statistics and sky subtraction. The 1σ error bar in the photometric calibration, which is the dominant source of random error in the M33 data, is shown near the upper left hand corner of each panel. The arrow shows the result of adopting $A_V = 1.4$ mag for the nucleus of M33, as measured by Gordon et al. (1999).

Fig. 13.— The $(J-H, H-K)$ TCD for the central regions of NGC 247, NGC 2403, and M33. The M33 measurements were made from images that were processed to match the distance and angular resolution of the NGC 2403 observations; these do not change greatly if measured from images processed to match the image quality of the NGC 247 data. Plotted are the luminosity-weighted colors within $0''.5$ (top panel) and between $0''.5$ and $1''.25$ (lower panel) of the center of each galaxy. Two points are plotted for M33 to show the sensitivity to extinction: one point assumes $A_V = 0.24$, as estimated by Pierce & Tully (1992), while the other assumes $A_V = 1.4$, based on the fit to the nuclear SED made by Gordon et al. (1999). The error bars show the uncertainty in the photometric calibration. Also plotted are data for (1) Galactic globular clusters, as listed in Table 5A of Brodie & Huchra (1990) and corrected for reddening using the $E(B-V)$ values listed in that table (crosses), (2) Magellanic Cloud SWB Type 1 and 2 clusters from Tables 4 and 5 of Persson et al. (1983) (filled triangles), and (3) the central regions of Sc galaxies, as listed in Table 4 of Frogel (1985). Frogel (1985) only corrected for foreground extinction, and the points plotted in Figure 13 have been corrected for internal disk extinction using the relation derived by Tully & Fouqué (1985) assuming $i = 45^o$. The arrow in the top panel connects the 1.5 Gyr and 3.0 Gyr [Fe/H] = 0 models from Worthey (1994), while the arrow in the lower panel connects the [Fe/H] = -0.22, [Fe/H] = 0, and [Fe/H] = 0.25 Worthey (1994) models with an age of 1.5 Gyr.

Fig. 14.— The $K-$band surface brightnesses of NGC 2403, NGC 247, and M33 as measured in concentric circular apertures. The dashed lines show the surface brightness profiles of M33 measured from data processed to simulate the appearance of the central field of this galaxy if viewed at the same distance and with the same angular resolution as NGC 247 and NGC 2403. Note that the mean central surface brightness of M33 is significantly higher than in the other galaxies. The error bars at the end points of the NGC 2403 and NGC 247 curves show the 1σ uncertainties due to photon statistics and sky subtraction.

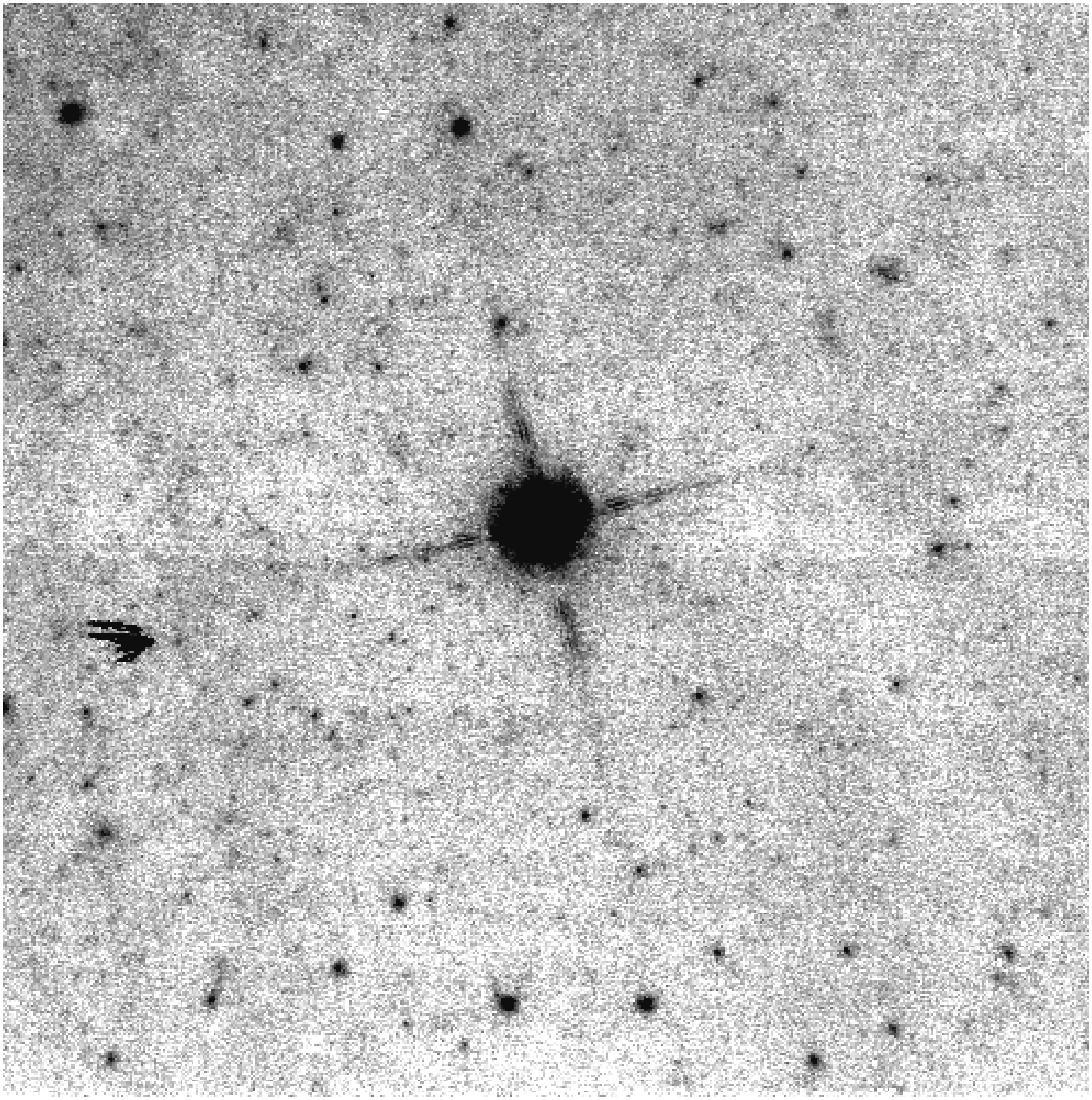

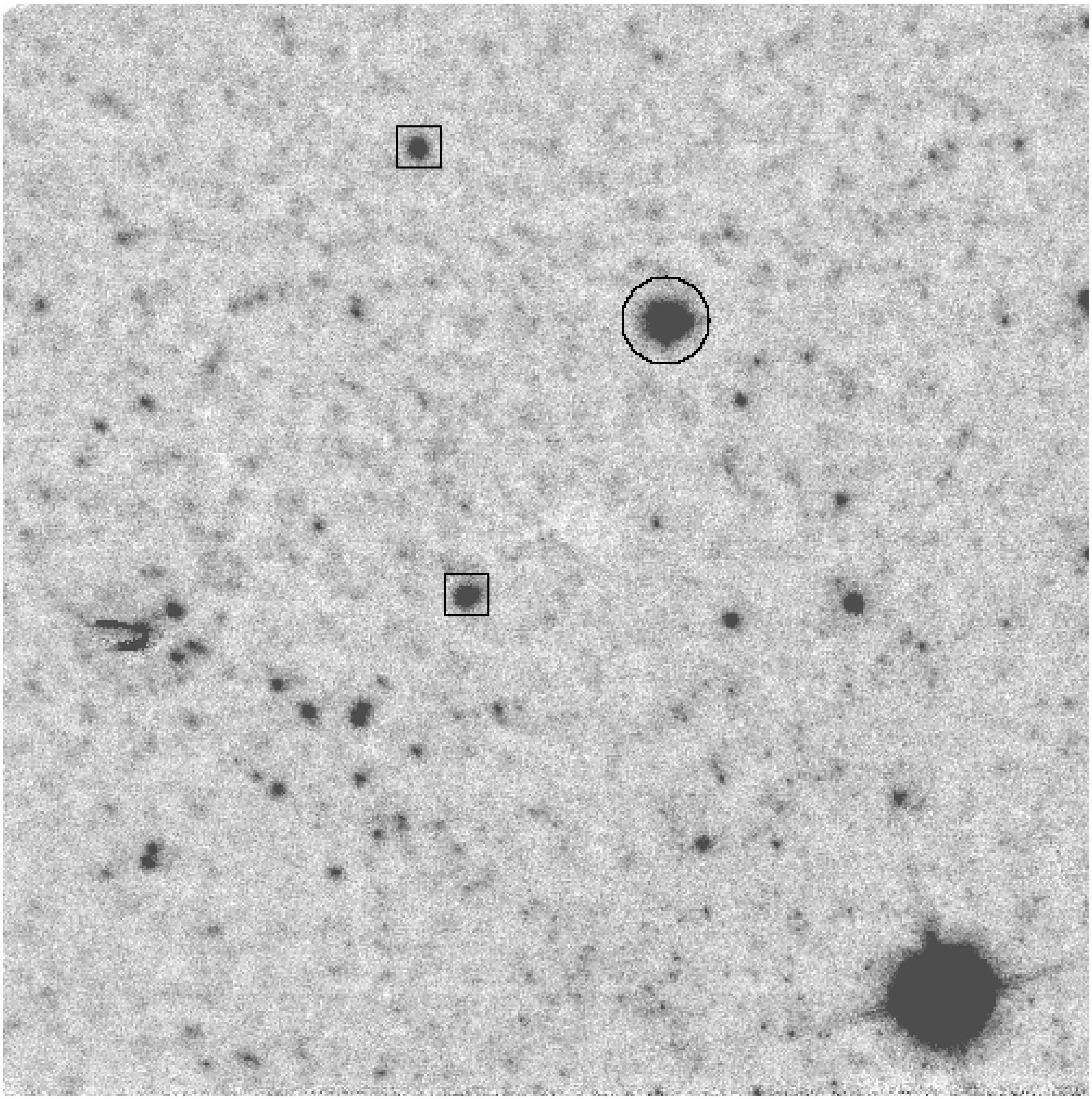

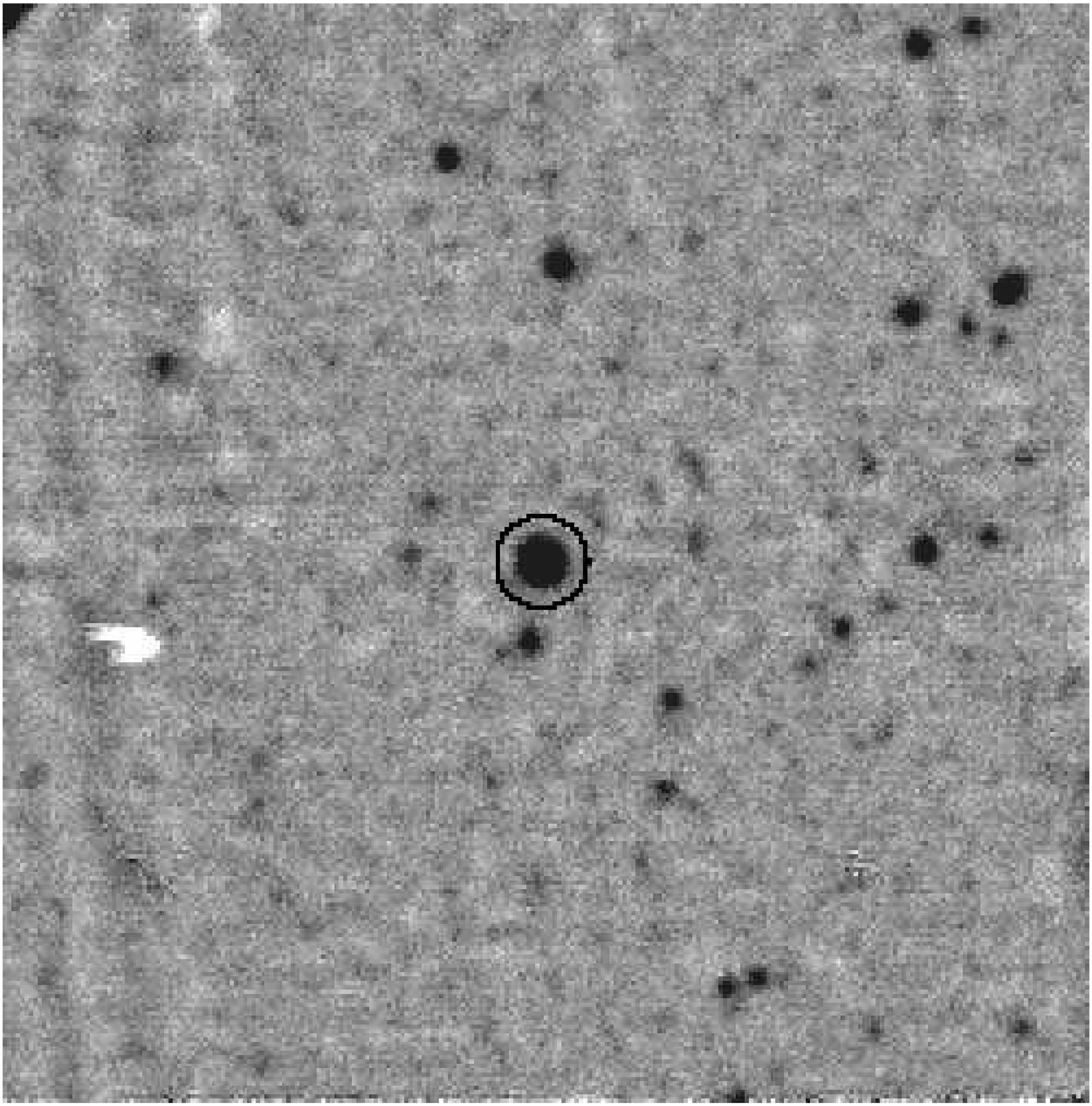

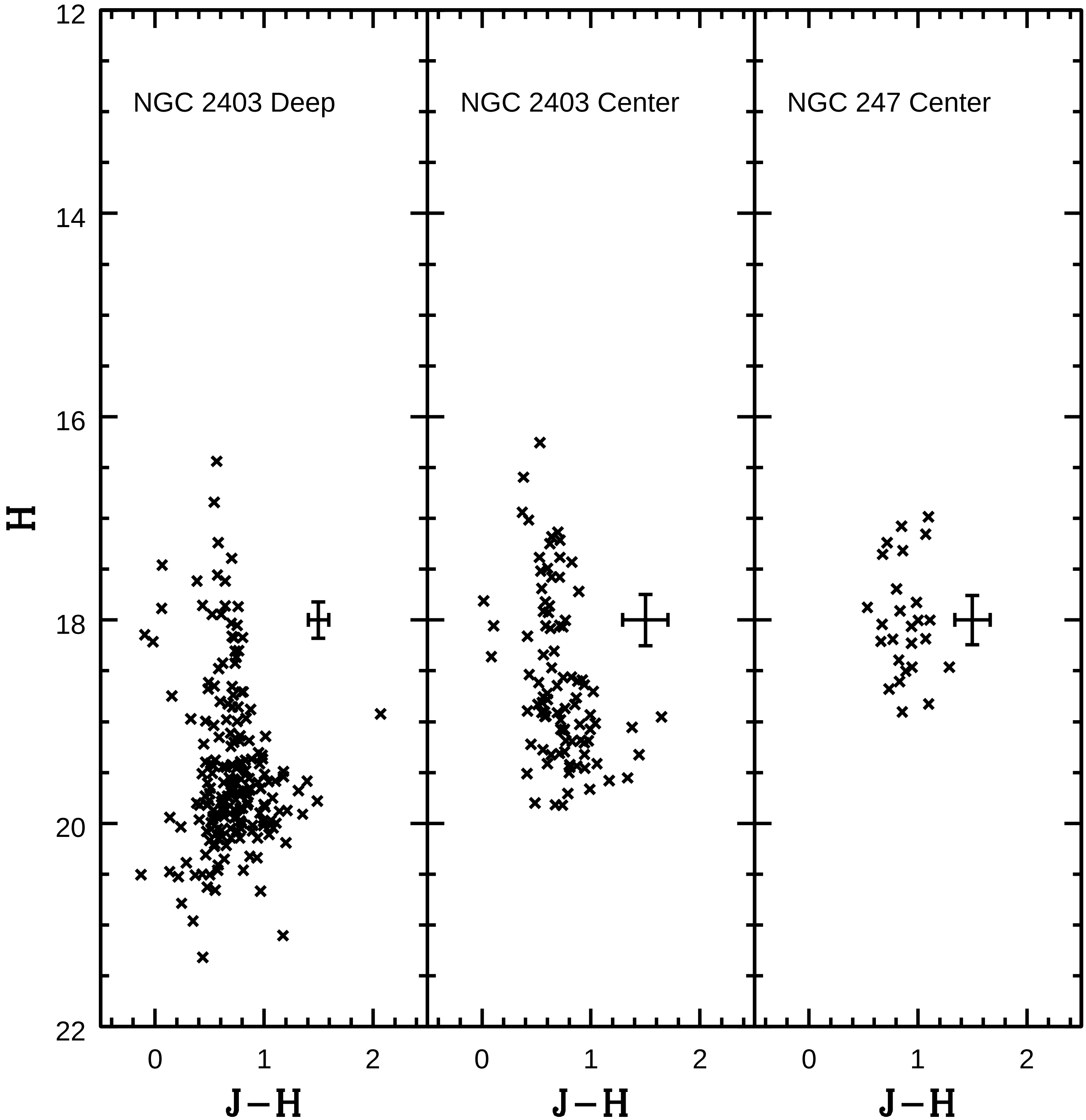

NGC 2403 Deep
NGC 2403 Center
NGC 247 Center
H
J−H
12
14
16
18
20
22
0
1
2

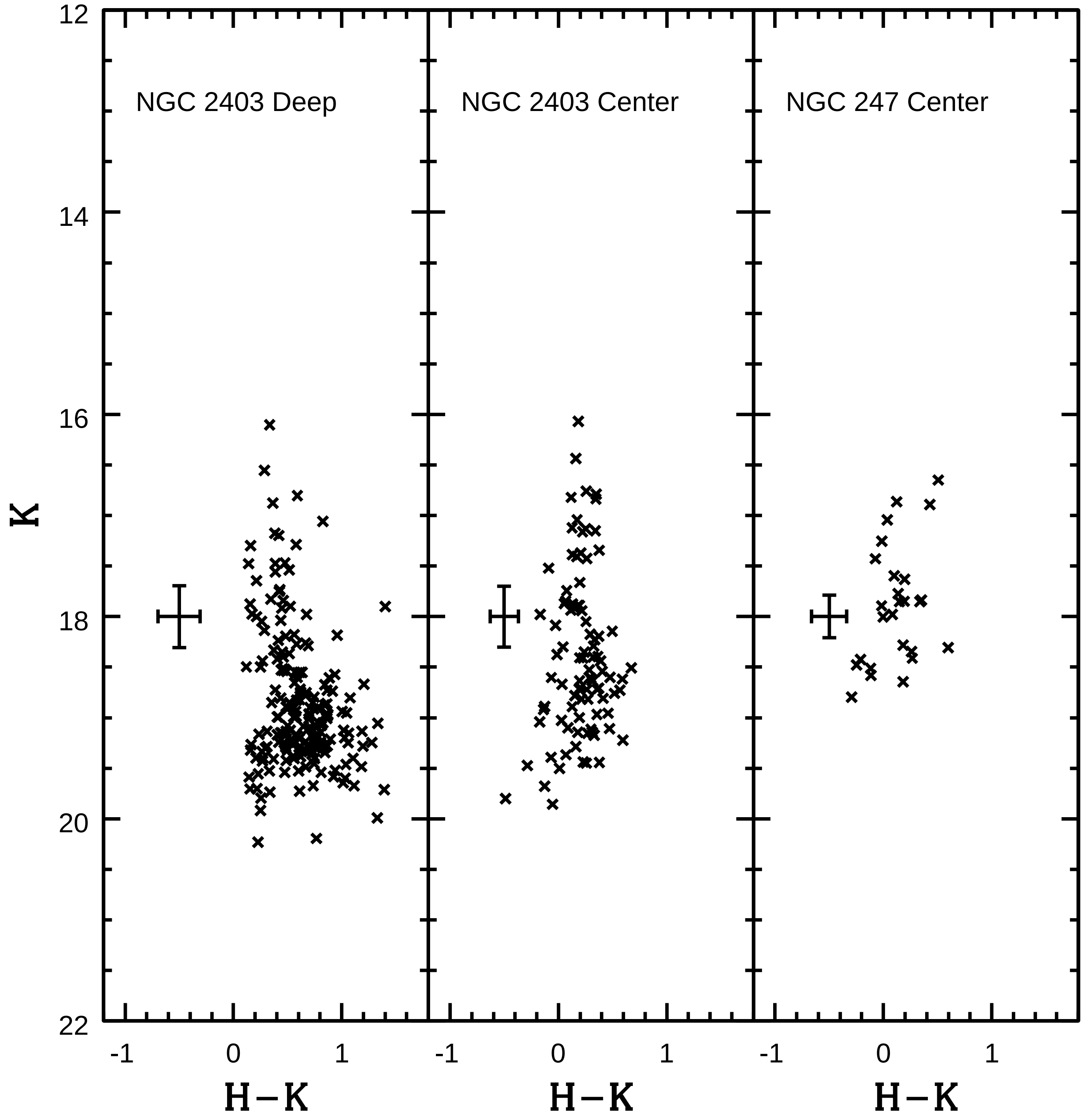
NGC 2403 Deep
NGC 2403 Center
NGC 247 Center
K
H−K
12
14
16
18
20
22
-1
0
1

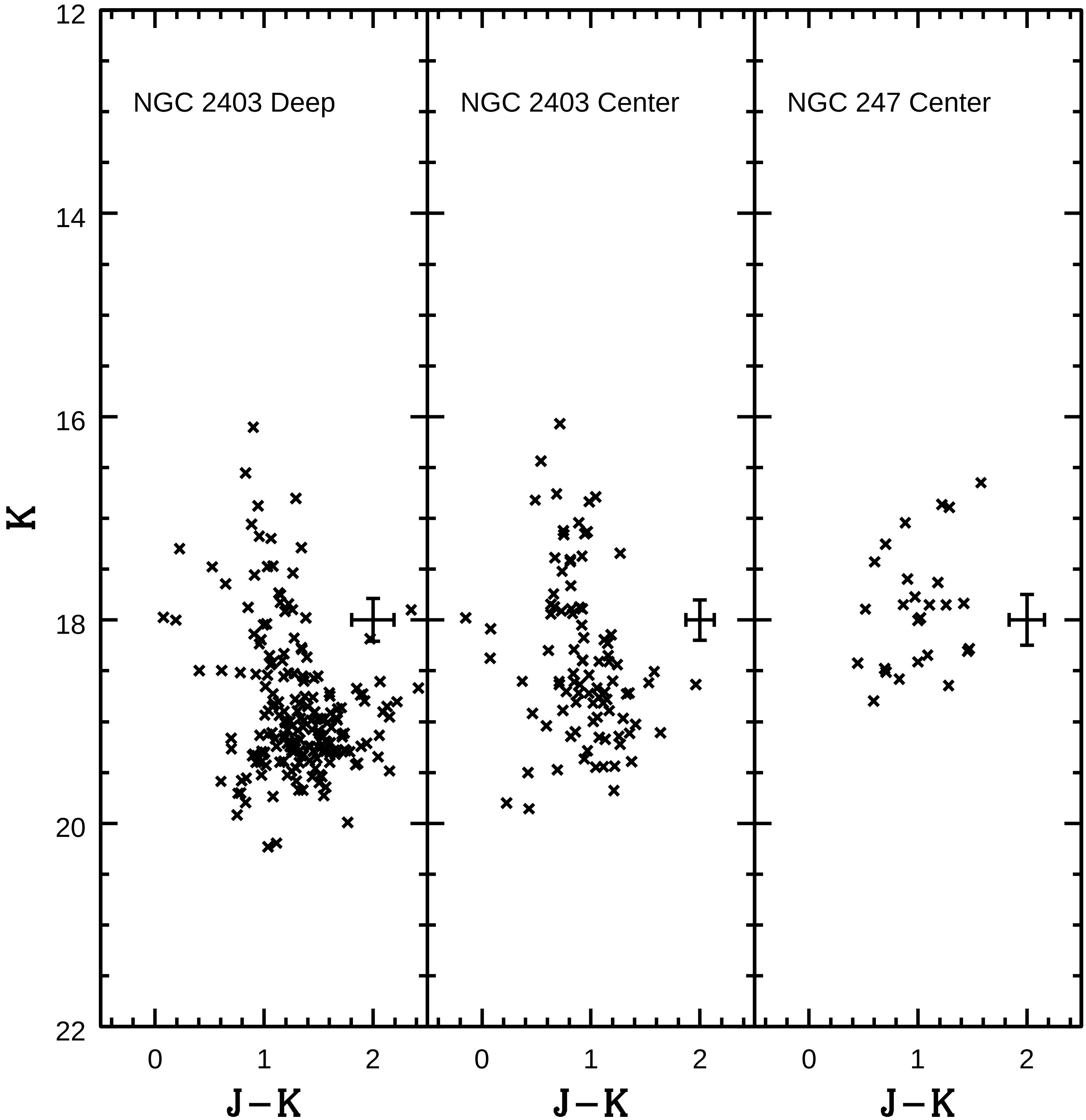
NGC 2403 Deep
NGC 2403 Center
NGC 247 Center
K
J−K
12
14
16
18
20
22
0
1
2

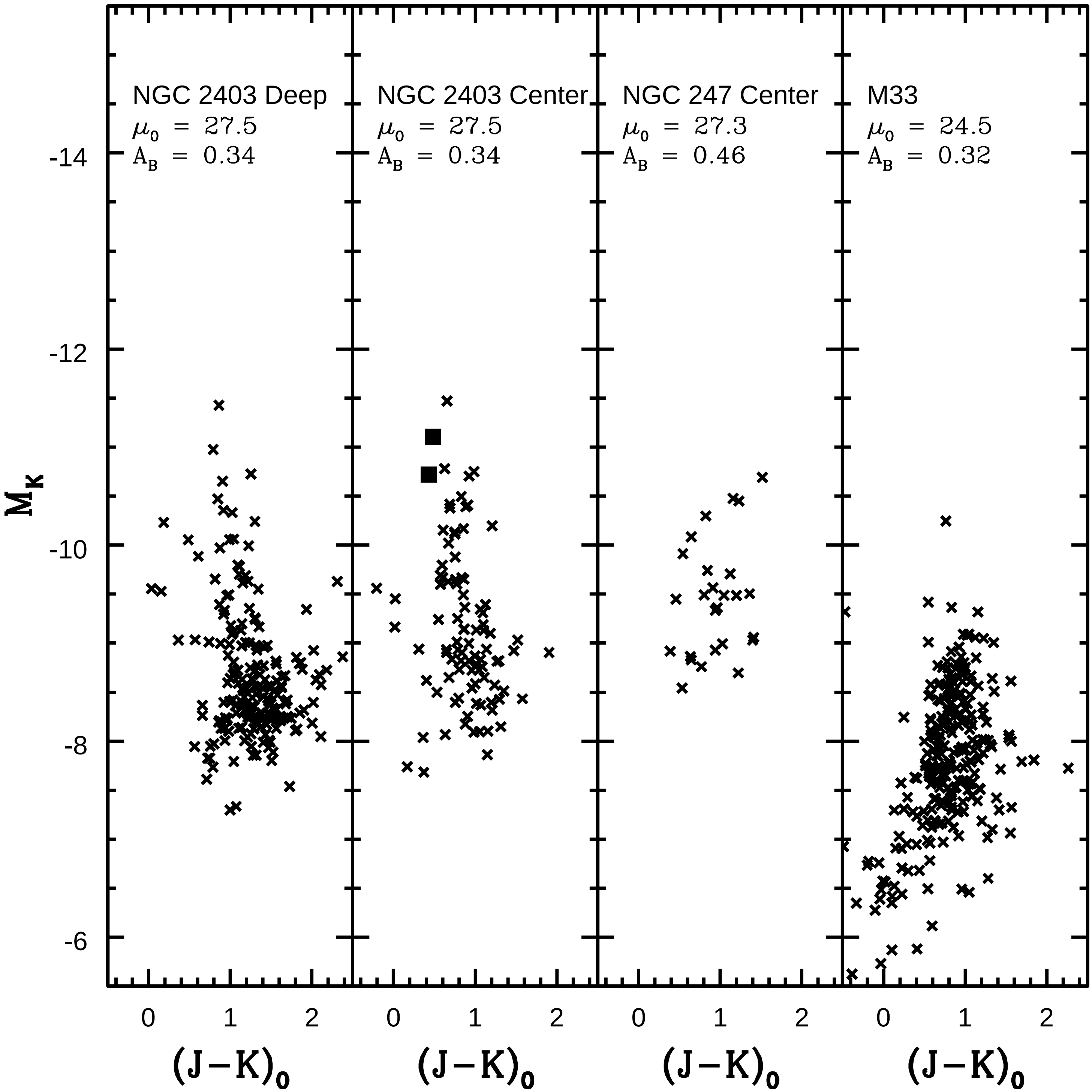
NGC 2403 Deep
μ_0 = 27.5
A_B = 0.34
NGC 2403 Center
μ_0 = 27.5
A_B = 0.34
NGC 247 Center
μ_0 = 27.3
A_B = 0.46
M33
μ_0 = 24.5
A_B = 0.32
-14
-12
-10
-8
-6
M_K
0
1
2
$(J-K)_0$

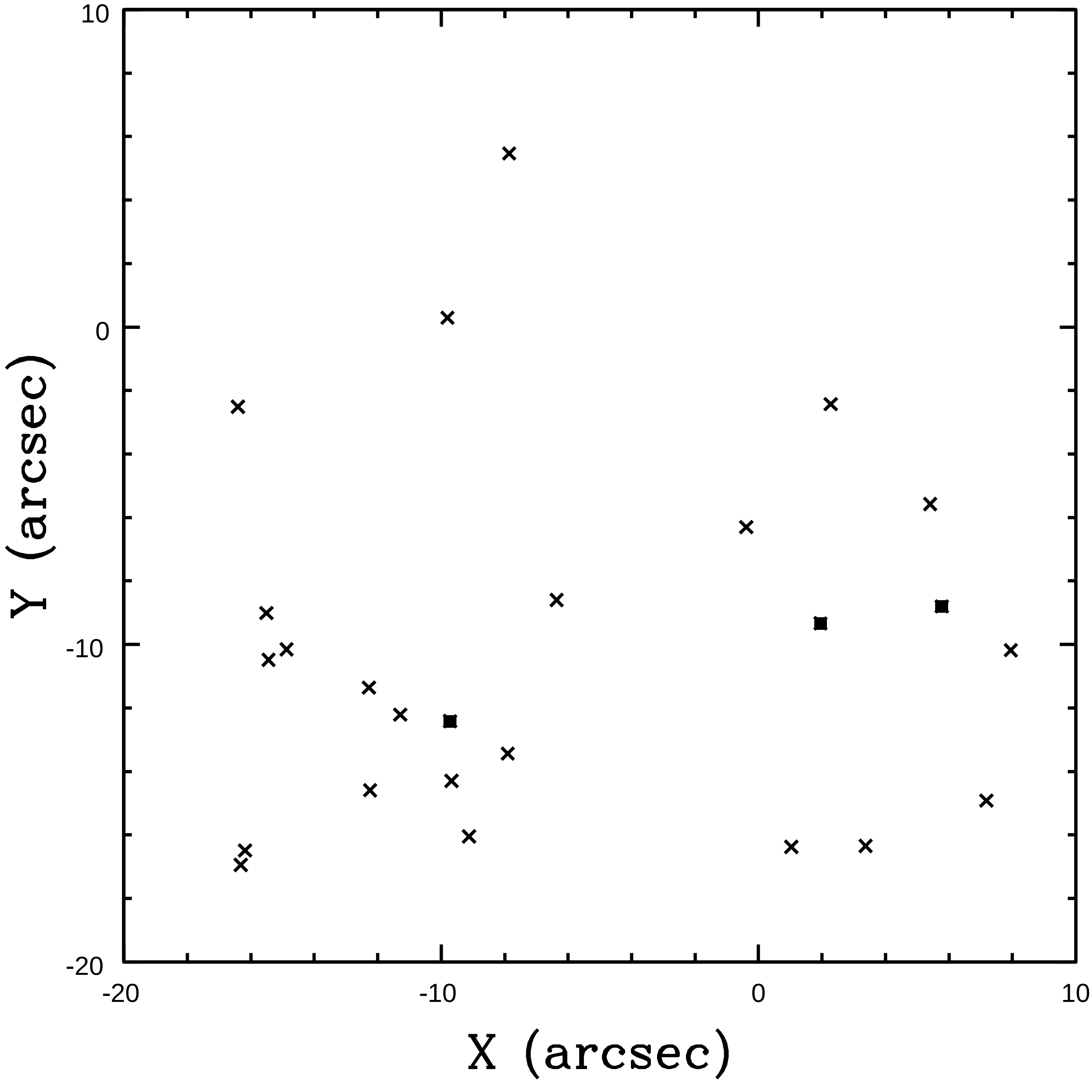
10
0
-10
-20
-20
-10
0
10
Y (arcsec)
X (arcsec)

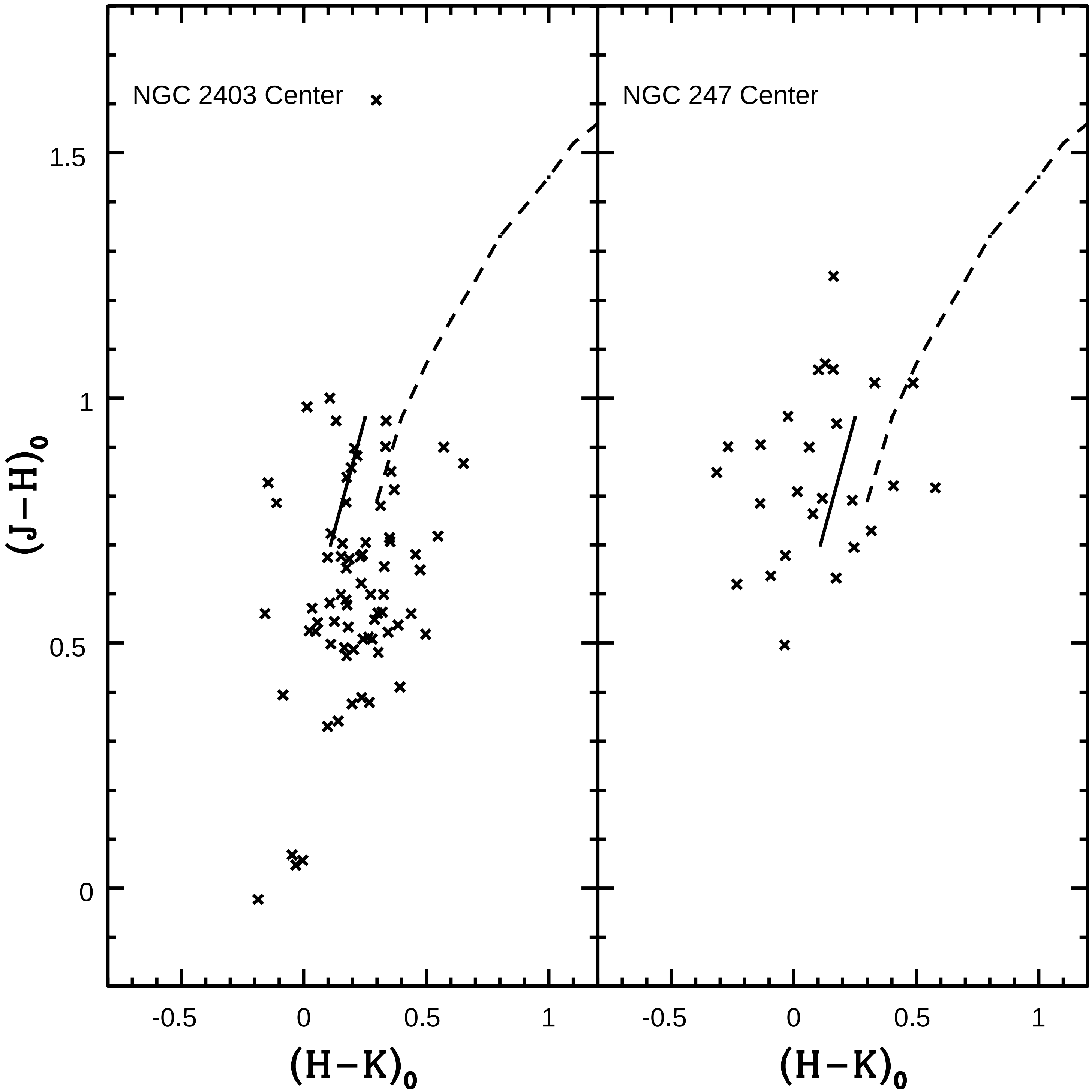
NGC 2403 Center
NGC 247 Center
(J−H)$_0$
(H−K)$_0$
1.5
1
0.5
0
-0.5
0
0.5
1
-0.5
0
0.5
1

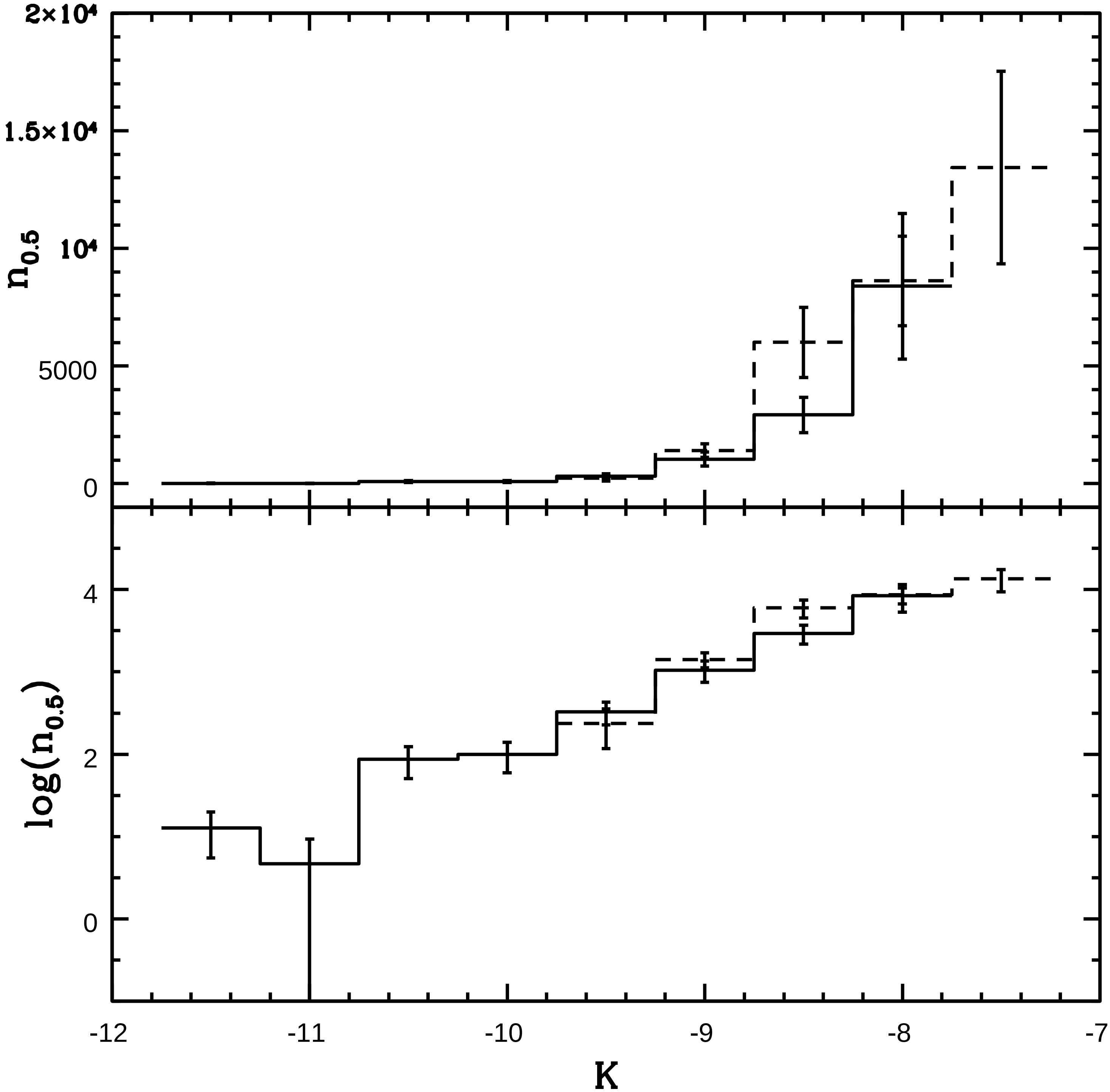

2×10⁴
1.5×10⁴
10⁴
5000
0
$n_{0.5}$
4
2
0
$\log(n_{0.5})$
-12
-11
-10
-9
-8
-7
K

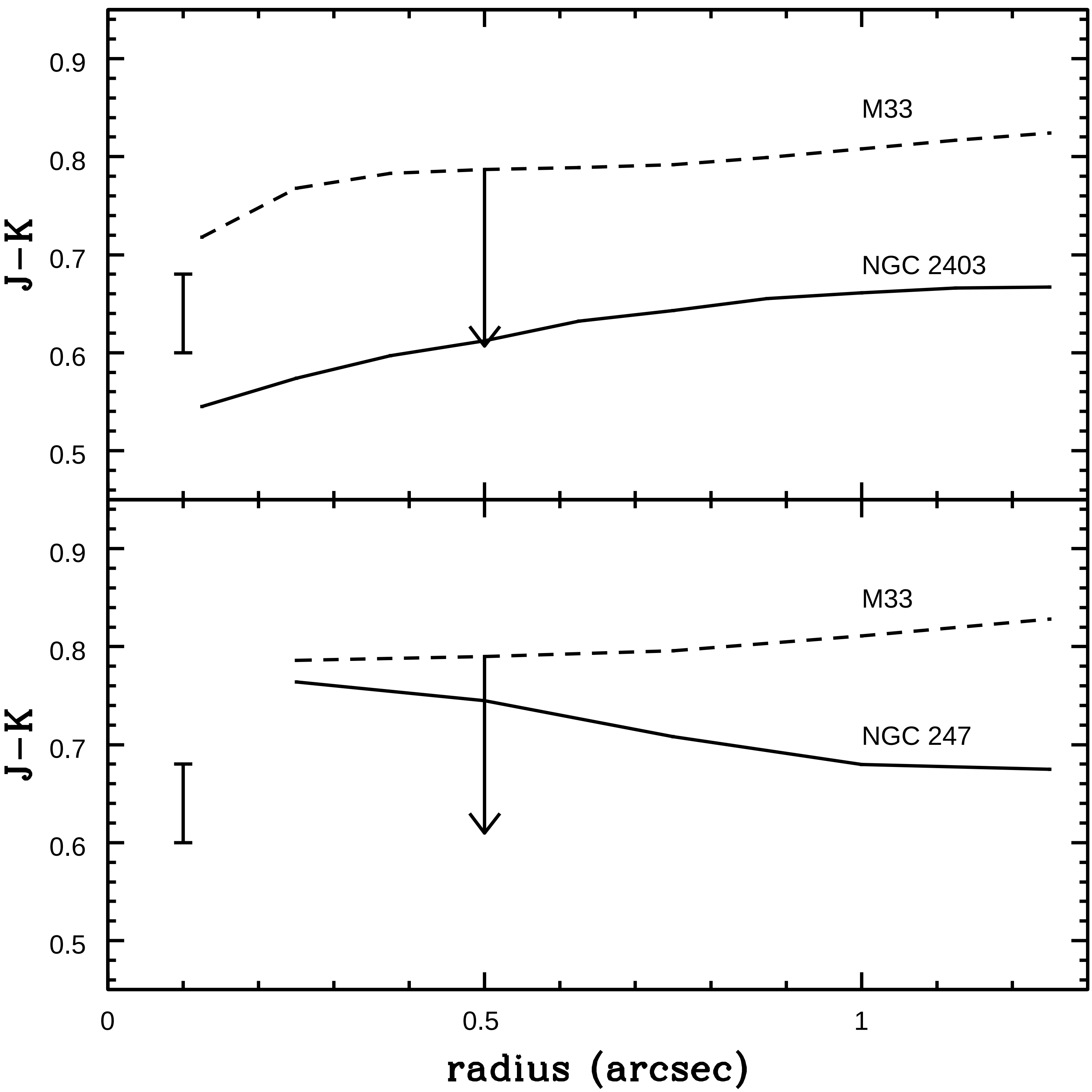

0.9
0.8
0.7
0.6
0.5
J−K
M33
NGC 2403
0.9
0.8
0.7
0.6
0.5
J−K
M33
NGC 247
0
0.5
1
radius (arcsec)

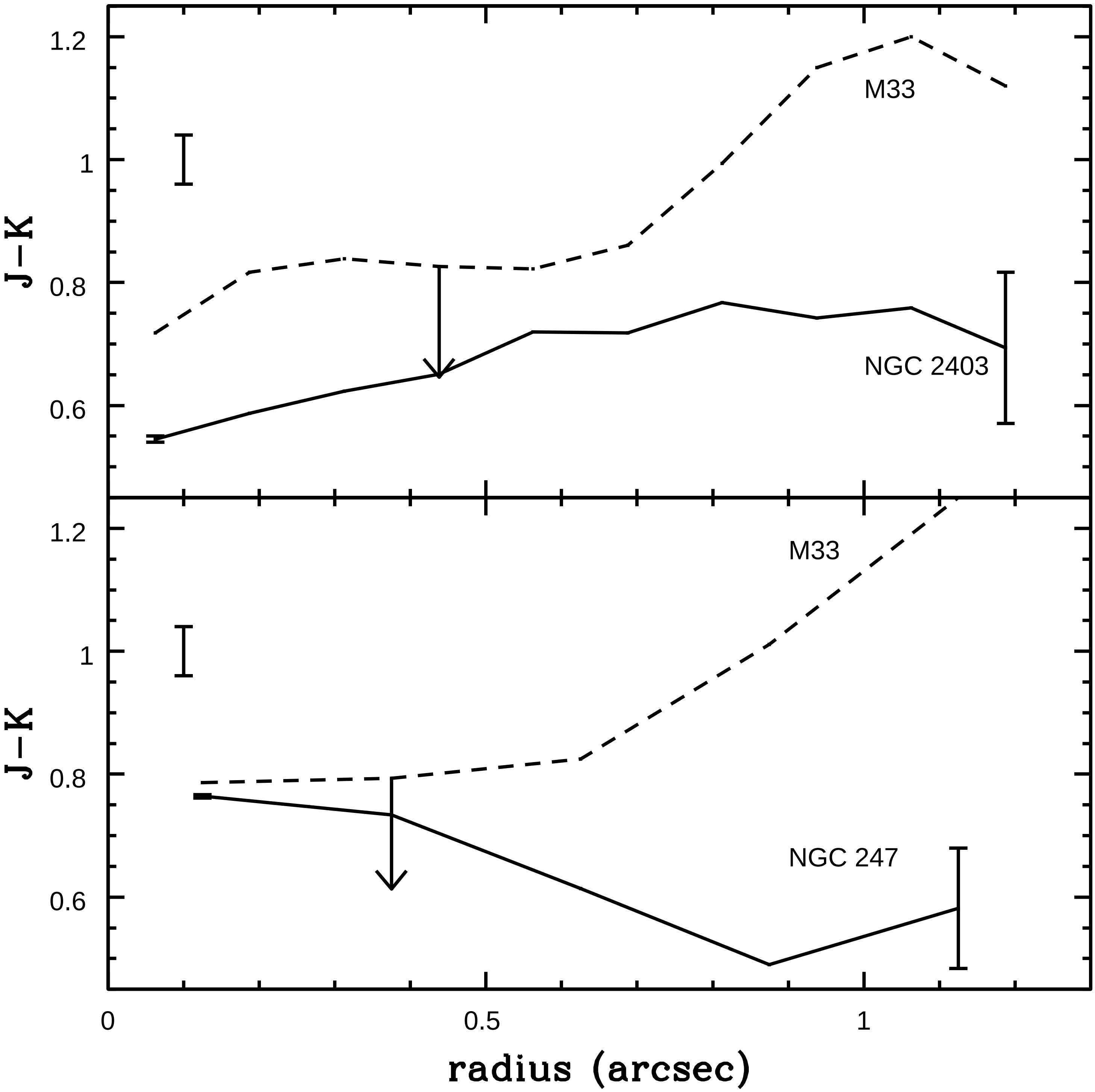

1.2
1
0.8
0.6
J−K
M33
NGC 2403
1.2
1
0.8
0.6
J−K
M33
NGC 247
0
0.5
1
radius (arcsec)

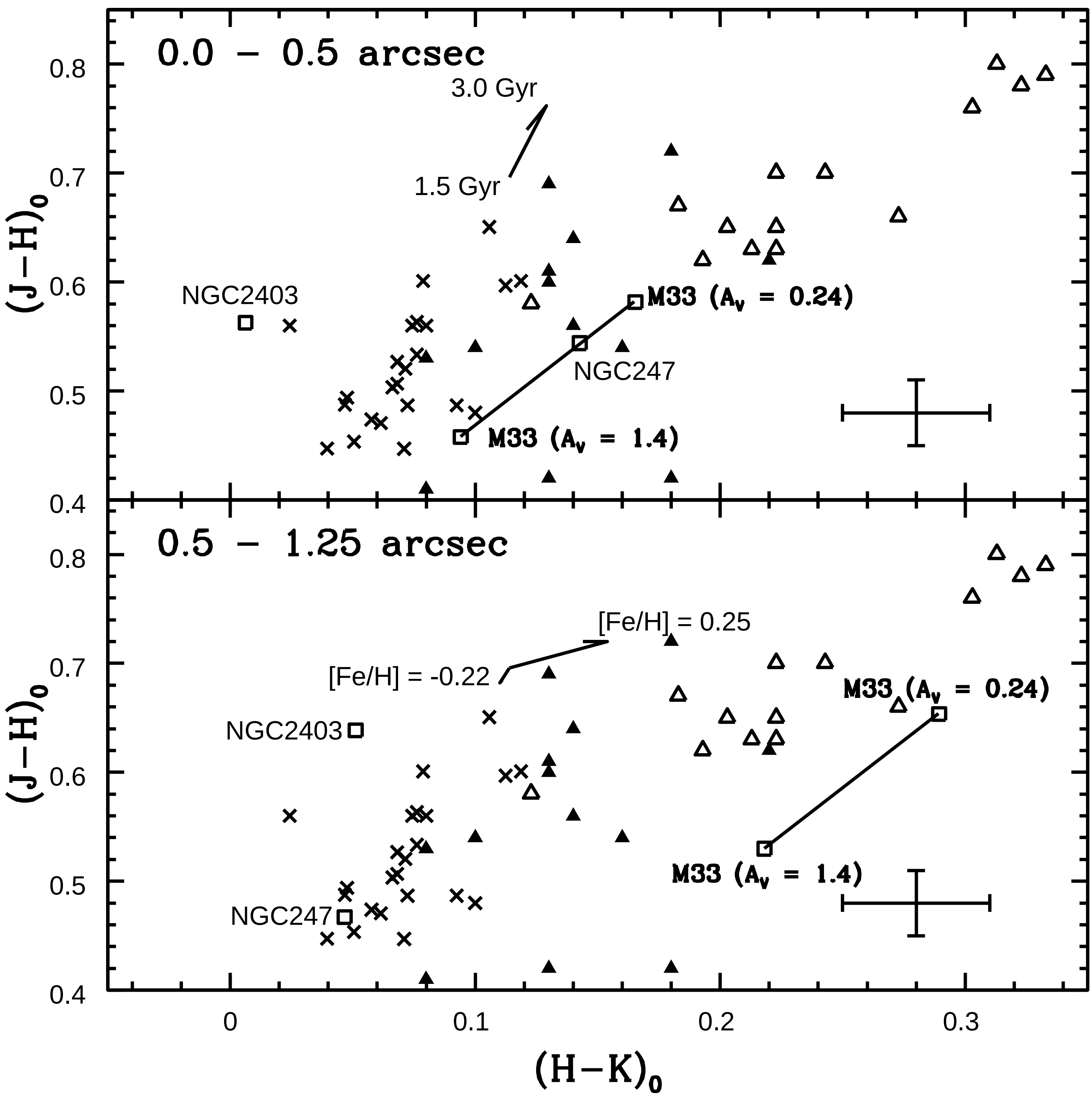

0.0 - 0.5 arcsec
3.0 Gyr
1.5 Gyr
NGC2403
M33 (A_V = 0.24)
NGC247
M33 (A_V = 1.4)
0.5 - 1.25 arcsec
[Fe/H] = 0.25
[Fe/H] = -0.22
NGC2403
M33 (A_V = 0.24)
M33 (A_V = 1.4)
NGC247
$(J-H)_0$
$(H-K)_0$
0.4
0.5
0.6
0.7
0.8
0
0.1
0.2
0.3

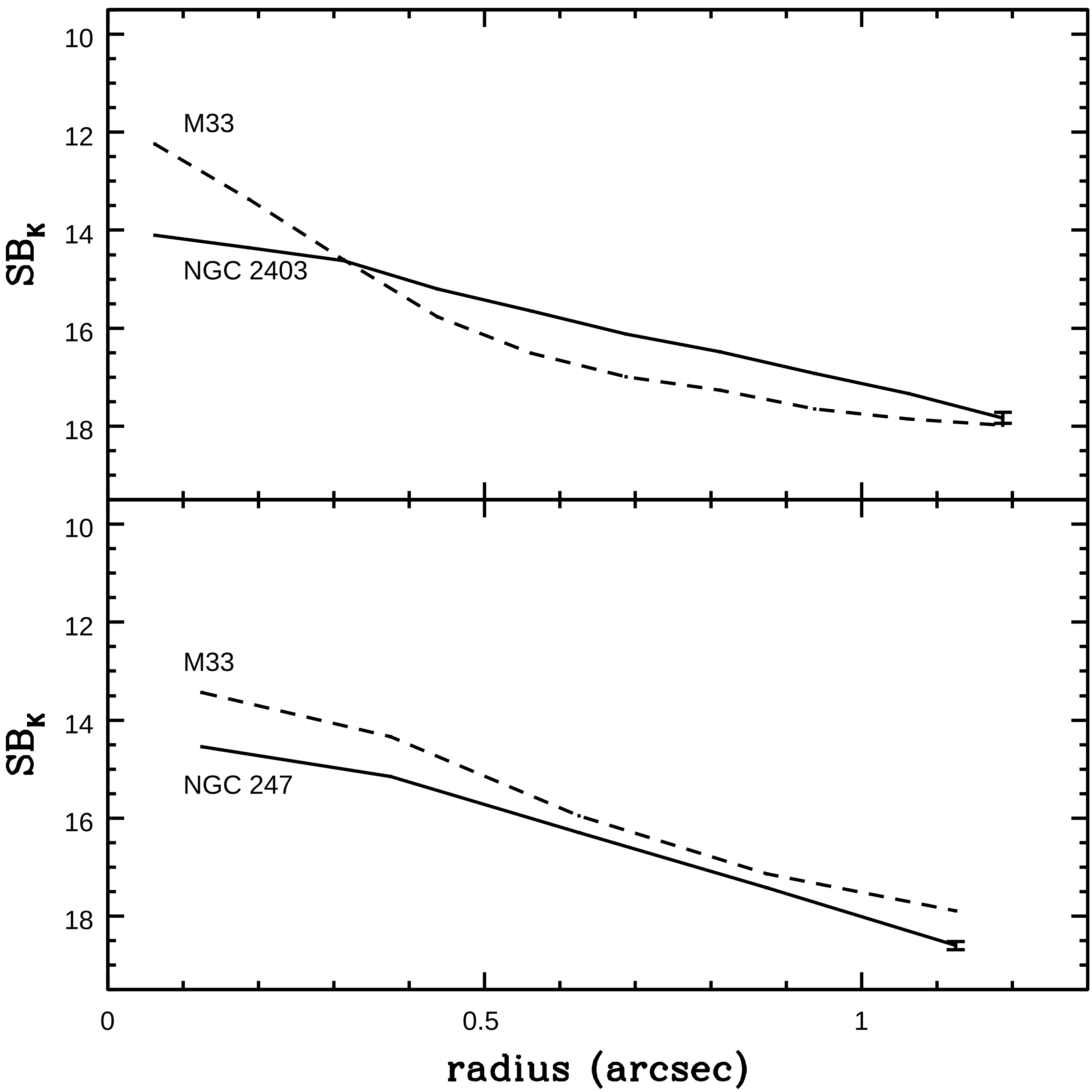

M33
NGC 2403
M33
NGC 247
SB_K
SB_K
10
12
14
16
18
0
0.5
1
radius (arcsec)